Chronology of the Late Roman Antiquity walls of Le Mans (France) by OSL, archaeomagnetism and radiocarbon

G. Hervé, P. Guibert, H. Meunier, M. Monteil, Ph. Dufresne, Ph. Lanos, C. Oberlin, G. Ben Aissa

Title

Chronology of the Late Roman Antiquity walls of Le Mans (France) by OSL, archaeomagnetism and radiocarbon

Authors with affiliations

G. Hervé (1), P. Guibert (2), H. Meunier (3,4), M. Monteil (5), Ph. Dufresne (2,6), Ph. Lanos (2,6), C. Oberlin (7), G. Ben Aissa (2)

(1) Laboratoire des Sciences du Climat et de l'Environnement/IPSL, UMR 8212, CEA, CNRS, UVSQ, 91191 Gif-sur-Yvette, France.
(2) Archéosciences Bordeaux, UMR6034, CNRS, Université Bordeaux Montaigne, Pessac, France.
(3) Service Archéologie, Direction générale adjointe Culture, Tourisme, Sport, Laval – Laval agglomération, Laval, France.
(4) CReAAH, UMR6566, CNRS, Le Mans Université, Le Mans, France.
(5) CReAAH-LARA, UMR6566, CNRS, Nantes Université, Nantes, France.
(6) Géosciences Rennes, UMR6118, CNRS, Université Rennes 1, Rennes, France.
(7) ArAr Archéologie et Archéométrie, UMR5138, CNRS, Université Lyon, Université Claude Bernard Lyon 1, Villeurbanne, France.

Abstract

The Late Roman Antiquity walls of Le Mans in northwest France are one of the most representative and preserved examples of the urban fortifications that developed in the Roman provinces of Gaul and Germany at this period. Because of a lack of reliable chronological data, the construction of the walls was poorly dated, which made unclear its historical context. The main objective of this study was to reassess the date of construction using several methods on a well-preserved sector (sector 11) of the Late Roman Antiquity walls. The dated masonries, thoroughly studied in building archaeology beforehand, are characterized by an alternating of stone and brick courses. Sampling focused on one hand on mortars with four radiocarbon dates (^{14}C) and six single-grain optically stimulated luminescence (SG-OSL) dates, and on the other hand on bricks with two OSL dates (quartz fine grain technique) and one archaeomagnetic date on a set of 104 bricks. The consistency between the dates on the two types of materials discards a possible reuse of the bricks from former Roman buildings. They were produced for the construction of the walls with the presence of several types of bricks likely reflecting a supply from at least two workshops. The dating program in the sector 11 also included 21 ^{14}C dates and six SG-OSL on protohistoric structures, Early Empire masonries and large medieval buildings, in order to investigate the evolution of the area over the long-term and to better constrain the chronology of the Late Roman Antiquity walls in Bayesian modelling. The chronological model (Chronomodel software) dates this construction between 301 and 423 CE at 95% of confidence. This date clearly excludes that the Late Roman Antiquity walls were built during the crises of the 3rd century, as previously thought, but rather in the stable political and economic context of the 4th century.

Keywords

Chronology; Late Roman Antiquity; urban wall; Gaul; OSL; archaeomagnetic dating; Bayesian modelling

1. Introduction

At the Late Roman Antiquity, cities in Roman Gaul underwent important transformations with a gradual decrease of their area from the end of the 2nd century CE and with the construction of walls in most capital cities between the last quarter of the 3rd century and the middle of the 5th century CE. This process is attested throughout the Roman Empire, the city of Rome itself being surrounded by a fortification from 270. In the provinces of Three Gauls and Germanies, the construction of such urban fortification is a new phenomenon, because almost all the capital cities did not have one during the Early Empire period. As elsewhere, it reflects major social and political changes in a context less stable than in the first two centuries CE. The period between ~230 and ~280 was actually characterized by multifaceted and successive crises in Gaul, as in the whole Roman Empire. Main factors were weakening of central power with a dissent in Gaul, coupled with first German incursions, brigandage, revolts, monetary inflation, epidemics and climate change with the end of the Roman Warm period. This troubled period was followed by a takeover of the Empire up to the end of the 4th century with an administrative and military reorganization, mainly by Aurelian (emperor in 270–275) then Diocletian (284–305) and Constantine (306–337), until the end of the 4th century (Sotinel and Virlouvet (eds), 2019).

In this changing historical context, the reason for the construction of urban fortifications and their role(s) in the cities remains unclear for most of them, because of chronological uncertainties. Building of urban walls were traditionally dated in the last third of the 3rd century, often around 270 CE at the climax of the crisis, giving them principally a defensive role. Archaeological excavations performed in several cities (e.g., Amiens, Grenoble, Reims, Tours) indicate that buildings in the Three Gauls and in Germanies occurred in reality over a longer period from the mid 3rd century up to the end of the 4th century. These reassessments suggest that urban walls, at least those built after 270, had also a promoting role of the regained power of the Empire and of the prestige of the city (Bayard and Fourdrin (eds), 2019; Intagliata et al., 2020).

This study focuses on one of the most famous examples of Late Roman Antiquity urban fortifications in Gaul, Le Mans in North-West France (48.0°N – 0.2°E) (Bouillet et al., 2022). At this period, the city was the capital of *Aulerci Cenomani* people in the *Gallia Lugdunensis* III province. The Late Roman Antiquity walls, built on a promontory above the Sarthe River, formed a NW-SE quadrangle of circa 500 × 100 meters, enclosing an area of 8.5 hectares (Fig. 1a). They are very well preserved over almost the three-quarters of the perimeter and sometimes over more than 10 m high. Their neat architecture is also famous with geometric patterns made by the assembly of different coloured rocks and bricks in the masonries. These characteristics, unique in Gaul, have attracted the interest of researchers since the 19th century. The most comprehensive study was performed by Joseph Guilleux in the 80-90s (Guilleux, 2000). Since, the development of rescue excavations and methodological improvements in building archaeology (e.g., 3D) have justified to resume in 2017 a global study of the walls in the framework of a Collective Research Program (*Projet Collectif de Recherche*) directed by two of us (MM & HM). After a first general study (Meunier and Augry, 2019), this program resulted in several publications (Bouillet et al., 2022; Meunier et al., 2022; Bocquet et al., 2022; Pithon et al., 2022) and an exposition in 2022-2023 at the archaeological museum of Le Mans (Jean-Claude Boulard – Carré Plantagenêt museum).

Precising the chronology of the fortification is one of the most important objectives of this project. The building of the Le Mans Late Roman Antiquity walls was previously fixed in 280±15 CE by archaeomagnetism on a set of 45 bricks (Goulpeau, 1985). But this first work suffered from several weaknesses. The main ones are the low number of bricks and the uncertainty on their original context, bringing doubt on its homogeneity and thus on the reliability of the dating (Lanos et al., 2015). The archaeomagnetic method has also considerably improved for 40 years in laboratory measurements, in the precision of reference curves and in the dating process thanks to Bayesian statistics (e.g., Lanos, 2004; Gallet et al., 2009; Le Goff et al., 2020; Brown et al., 2021). Moreover, archaeomagnetism date the production of the bricks and not the construction of the wall itself, while the reuse of materials from older building was assumed common at the Late Roman Antiquity.

The main objective of our study is to reassess the date of the construction of the urban walls in the light of recent improvements in dating techniques applied to building archaeology. For a few years, the construction of a masonry can now be directly dated by "single-grain" optically stimulated luminescence (SG-OSL), applied to the quartz grains extracted from lime mortar (e.g., Goedicke, 2011; Urbanová and Guibert, 2017; Urbanová et al., 2018; Guibert and Urbanová, 2022). Another major step forward is the development of hierarchical Bayesian modelling to synthesize multiple dating results in integration with archaeological information as stratigraphic constraints (e.g., Buck and Millard, 2004; Bronk Ramsey, 2009; Lanos and Dufresne, 2012). Using this statistical approach, we provide here a new estimation of the construction of Le Mans urban fortification thanks to the acquisition of new radiocarbon and SG-OSL dating results on mortars and of new archaeomagnetic and OSL dating results on bricks. This strategy to study both types of materials gives also the opportunity to investigate the possible reuse of older bricks, providing information on the building economy. Such multidisciplinary integrated dating program has already been performed, mostly on religious buildings from the Early Middle Age (e.g., Bailiff and Holland, 2000; Bailiff, 2007; Guibert et al., 2012; Stella et al., 2013; Urbanová et al., 2018, in press; Panzeri et al., 2019, 2020) and more rarely on Roman buildings (Urbanová et al., 2015, 2016), but it is, to our knowledge, unprecedented on Late Roman Antiquity urban fortifications. Finally, our chronological study aims to better define the evolution in time of the Le Mans Late Roman Antiquity walls at the medieval period. In spite of the construction of new buildings leaning on the walls, these one maintained their defensive function through the centuries and no important new fortification was built in Le Mans before the mid-14th at the beginning of the Hundred Year's war (Bouillet et al., 2022).

2. Archaeological context

The sector 11 in the south-eastern part of the Roman walls is a key area to fulfil these different objectives (Fig. 1b-c). It has the advantage to present a well-preserved section of the Late Roman Antiquity urban fortification, a few Early Empire architectural remains and large medieval

buildings belonging to the former residence and collegiate church of the Counts of Maine, which allows to investigate the evolution of this area over the long term (Meunier and Monteil, 2019a, 2020; Bouillet et al., 2022). The absence of large restoration and an easy access to the different buildings also facilitated the detailed study of this sector in building archaeology.

2.1 General description of the sector 11

The Late Roman Antiquity urban walls are mainly preserved in the Pierre de Ronsard garden with a courtine, called section 11-300, of almost 15 m in length and 7.5 m in height (Fig. 1d). Smaller portions of the walls are also visible in the cellars of the city hall (Fig. S1a-b-c-d in supplementary material). In this sector, the wall itself is numbered 11108 and its foundations 11109. These foundations are made either with large stone carved blocks likely in reuse from Early Empire buildings as in the section 11-300 (Fig. 1d), or with mixed smaller rubbles in an orange-coloured lime mortar (Fig. S1a). Above, on the facade, the masonry presents an alternating of brick courses, each one composed of three layers, and of rubble courses mainly in a local purple sandstone ("roussard" sandstone) (Fig. S1a-b-d). These materials are embedded in a crushed *terracotta* mortar (i.e., a lime mortar with sand and crushed *terracotta* in frequent use at the Roman period). The inner part of the wall, apparent thanks to the digging of a medieval gallery (GAL11103, Fig. S1b-d), is constituted by "roussard" sandstone rubbles and a few brick fragments embedded in a beige lime mortar (Fig. S1b-d).

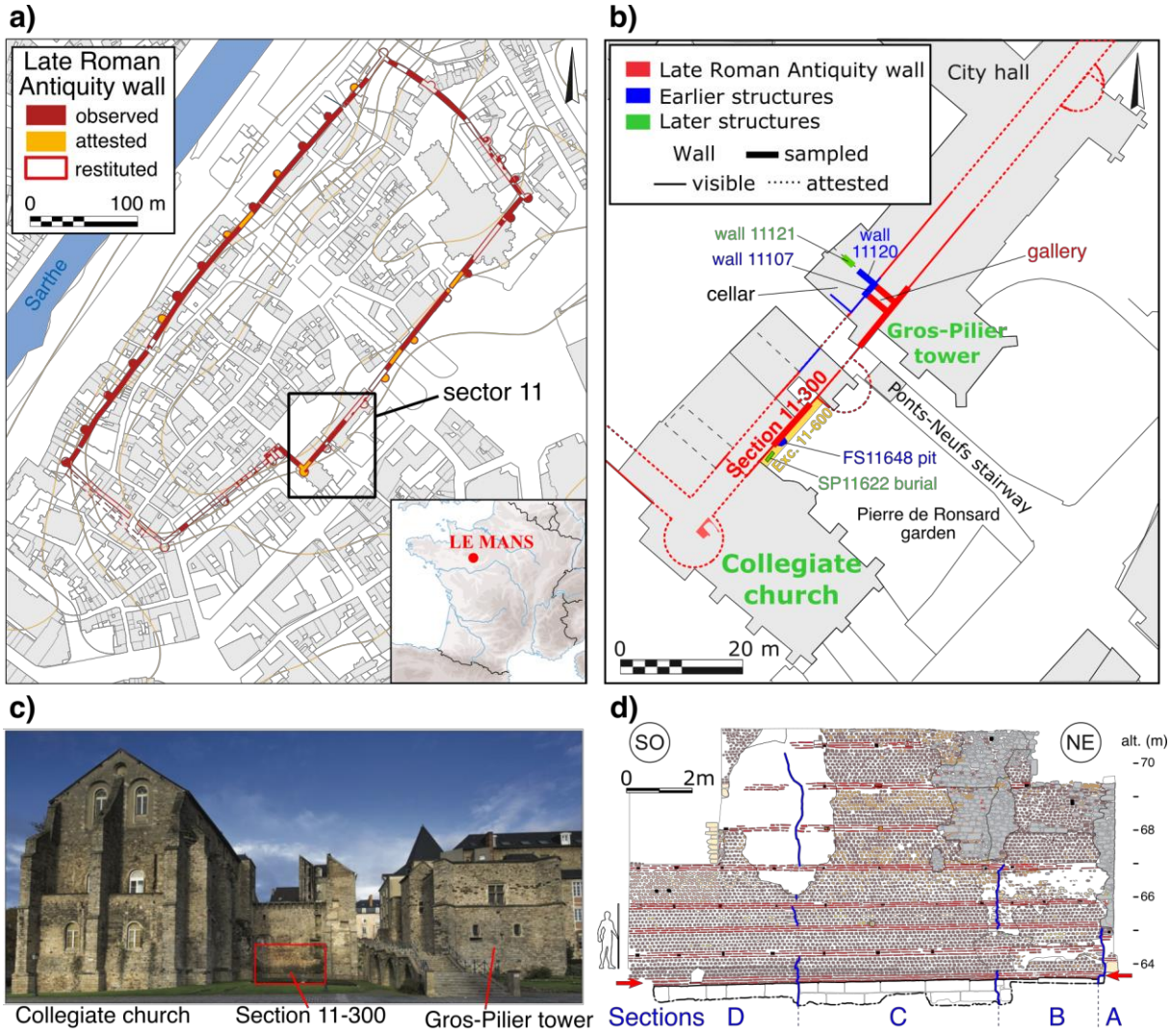

Figure 1: (a) General plan of the Late Roman Antiquity urban fortification at Le Mans. (b) Plan of the sector 11 highlighting sampled walls and structures. (c) View of the sector 11 from South-East i.e. from outside the Roman walls. (d) Drawing of the section 11-300. The red arrows indicate the lowest brick course sampled for the archaeomagnetic study. (From Meunier and Monteil, 2019b, 2020; CAD: H. Meunier)

The courtine 11-300 gives an insight on the building method (Meunier and Monteil, 2019b). Its careful observation revealed that it was constructed in four successive sections, named A-B-C-D, on the entire height of the wall (Fig. 1d). Their connections in the masonry indicate that the sections A and D were the first built, then C and finally B. The used materials and building techniques (position of geometric patterns and putlog holes) slightly differ between sections,

158 suggesting temporary breaks in the construction or the implication of several team workers. Two
159 sizes of bricks are for example observed (Nauleau, 2019). Bricks with a 260 × 320 mm modulus
160 were used in sections B and D, whereas bricks from the section C have a similar thickness (35-40
161 mm) but a larger 280 × 380 mm modulus. This spatial distribution can be explained by a supply
162 at different workshops or by the reuse of one type of bricks. As the size of brick seems to decrease
163 through the Roman period in Gaul (e.g., De Filippo, 2004; Nauleau, 2013), one could especially
164 wonder if bricks of large modulus were not collected on an older building for the construction of
165 the courtine.

166 Actually, remnants of buildings older than the fortification are present nearby. Two portions of
167 walls, named 11107 and 11120, can be observed in the cellar of the city hall (Fig. S1b-c-d). The
168 analysis of their lime mortar shows that they belonged to two different construction stages or to
169 two different buildings. According to building archaeology, the wall 11120 is, likely slightly,
170 posterior to the wall 11107. These two walls likely date from the Early Empire period and were
171 associated to a public building. A short portion of a third wall, 11121, is also visible in this cellar
172 (Fig. S1b). A modern door prevents to know its temporal relationships with the walls 11107 and
173 11120 as well as with the Late Roman Antiquity urban fortification. The archaeological
174 interpretation suggests that this wall 11121 is more recent than the fortification, but this
175 hypothesis requires confirmation and, in this study, we consider that its date is undetermined.

176 In the sector 11, the medieval period was characterized by the construction of the Counts of Maine
177 residence, at the location of the modern city hall and whose main remains are today the Gros-
178 Pilier tower and the Saint-Pierre-de-la-Cour collegiate church (Fig. 1c). While the Gros-Pilier
179 tower was built in the 15th century, the chronology of the collegiate church is less well-known. Its
180 most recent parts, the choir, was built in the 13th-14th centuries as indicated by historical sources
181 and dendrochronology. Conversely, the building of the nave, a tower and an arcade overlain by
182 the choir did not have any dating elements until recently (Meunier and Monteil, 2019a).

Besides building archaeology investigations, the occupation of the area is known by an excavation (excavation 11-600) performed in 2019 at the base of the courtine 11-300 (Fig. 1b) (Meunier and Monteil, 2020). The deepest stratigraphic feature is a pit or a ditch (FS11648) of which the absence of Roman ceramics in the filling layers suggests a protohistoric dating. This pit is covered by backfill layers and by a circulation layer dated in the beginning of the 1st century CE. The stratigraphic unit above is an *in-situ* layer of crushed *terracotta* mortar related to the construction of the Late Antiquity walls. The absence of layers between the mortar unit and the 1st century backfill layers reflects earthwork immediately before the construction. The mortar layer does not appear eroded and the deposition of a short sequence of dark earth (unit 11625) just above likely occurred shortly after the construction of the fortification. Very interestingly, this unit 11625 contained two dated artefacts, first a Crispus coin, a *nummus* coin minted at Lyon in 318-319 (pers. comm. Gérard Aubin). The second artefact is a rim of a Chenet 320 cup in Argonne sigillata dated in the middle or the second half of the 4th century (pers. comm. Christian Le Boulaire). Just below the modern soil, the stratigraphy ends by two Early Middle Age burials (SP11622 and SP11654) (Meunier and Monteil, 2019b, 2020, 2021; Bouillet et al., 2021).

2.2 Dating strategy

The dating strategy was defined to optimize Bayesian chronological modelling. The Late Roman Antiquity wall was the most sampled structure, because the reassessment of its construction constituted the main objective of the study. Mortars were dated by SG-OSL on quartz grains and by radiocarbon on charcoal inclusions. Bricks were also studied for archaeomagnetic and multigrain OSL dating. Unlike dates on mortars, these methods do not date the construction but the production of the bricks and the comparison between the two materials allows to investigate the possibility of a reuse of bricks from older buildings. In order to better understand the course of the construction, we sampled the wall itself (wall 11108), its foundations (wall 11109) and the different sections of the courtine 11-300.

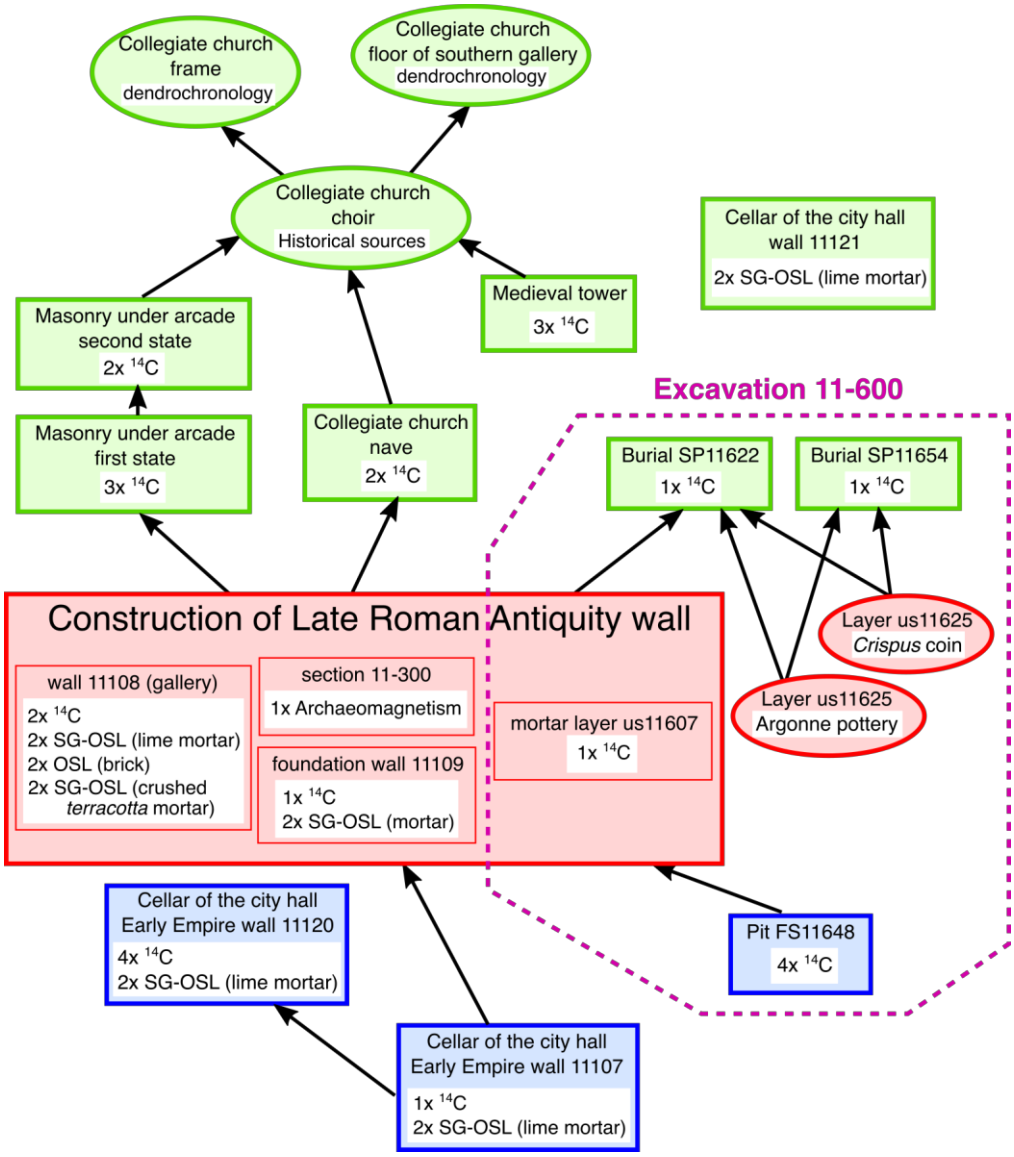

Figure 2: Simplified stratigraphic diagram of studied contexts with the number of obtained dates. The diagram reproduces the formalism of Chronomodel software (Lanos and Dufresne, 2019). Rectangular boxes correspond to dated events, while circular boxes indicate *Termini Ante Quem* and *Post Quem* (called bounds in Chronomodel). The structures related to the construction of the Late Antiquity Roman wall are in red, those before the construction in blue and those posterior to the construction in green.

As the precision of a Bayesian model is improved by the integration of anteriority or posteriority relationships, dating was not limited to the Late Roman Antiquity wall but also considers earlier

and medieval buildings, as well as structures of the excavation 11-600. In total, our experimental work includes 25 radiocarbon dating (22 on charcoals and 3 on bones), 12 SG-OSL dating on mortars, two OSL dating on bricks and one archaeomagnetic dating on a large set of bricks. The sampled contexts are summarized in the Table 1 and Figure 2 together with other chronological information available in the sector 11 provided by stratigraphy, dendrochronology and historical sources. The location of samples is presented in Figures S1 and S2 in supplementary material.

Table 1: Summary of chronological data. Context: location of the sample; Dating method; Dated material or artefact; Laboratory number of the sample for physical dating techniques; Results before calibration for physical dating techniques: uncalibrated age with 1σ standard deviation for ^{14}C, age in years before year of measurement with 1σ standard deviation for OSL, average inclination with radius of the 95% confidence circle (α_{95}), precision parameter (k) and number of bricks for archaeomagnetism; Date intervals.

Context	Method	Material	Lab. number	Results	Intervals (Cal yrs CE)
After construction of the Late Roman Antiquity wall					
Collegiate church, floor of southern gallery in the choir					
	Dendrochronology	wood	DT-2019-072		1487-1488
Collegiate church, frame of the choir					
	Dendrochronology	wood	DT-2019-072		1330-1334
Collegiate church, choir					
	Historical sources				after 1267
Collegiate church, nave					
	^{14}C	charcoal	Lyon-14077(RICH)	1045±30 BP	[897; 922] (8%), [953; 1036] (87%)
	^{14}C	charcoal	Lyon-14078(RICH)	1056±30 BP	[896; 924] (14%), [950; 1031] (81%)
Medieval tower					
	^{14}C	charcoal	Lyon-15767(GrM)	970±30 BP	[1022; 1158] (95%)
	^{14}C	charcoal	Lyon-15768(GrM)	1040±30 BP	[897; 922] (6%), [953; 1039] (89%)
	^{14}C	charcoal	Lyon-15769(GrM)	965±30 BP	[1024; 1158] (95%)
Masonry under arcade, second state					
	^{14}C	charcoal	Lyon-15773(GrM)	965±30 BP	[1024; 1158] (95%)
	^{14}C	charcoal	Lyon-15774(GrM)	1030±30 BP	[900; 917] (3%), [975; 1047] (87%), [1084; 1147] (5%)
Masonry under arcade, first state					
	^{14}C	charcoal	Lyon-15570(GrM)	940±30 BP	[1029; 1174] (95%)
	^{14}C	bone fragment	Lyon-15571(GrM)	1170±30 BP	[775; 899] (73%), [917; 974] (22%)
	^{14}C	charcoal	Lyon-15572(GrM)	970±30 BP	[1022; 1158] (95%)
Excavation 11-600, burial SP11622					
	^{14}C	bone	Lyon-17993(GrM)	1445±30 BP	[574; 651] (95%)
Excavation 11-600, burial SP11654					
	^{14}C	bone	Lyon-17994(GrM)	1090±30 BP	[891; 996] (87%), [1003; 1020] (8%)
Undetermined period, cellar of the city hall, wall 11121					
	SG-OSL	lime mortar	BDX22226	2629±175 (meas. in 2019)	-610±175 (1σ)
	SG-OSL	lime mortar	BDX22227	1973±179 (meas. in 2019)	46±179 (1σ)
Associated to construction of the Late Roman Antiquity wall					
Late Roman Antiquity wall, gallery between the cellar of the city hall and the Gros-Pilier tower room, wall 11108					
	^{14}C	charcoal	Lyon-14074(RICH)	1675±30 BP	[257; 282] (12%), [328; 433] (81%), [467; 473] (1%), [518; 528] (1%)
	^{14}C	charcoal	Lyon-14075(RICH)	1750±30 BP	[240; 402] (95%)
	SG-OSL	lime mortar	BDX22216	1553±173 (meas. in 2019)	466±173 (1σ)
	SG-OSL	lime mortar	BDX22217	1553±128 (meas. in 2019)	466±128 (1σ)
	OSL	brick	BDX22220	1762±107 (meas. in 2019)	257±107 (1σ)
	OSL	brick	BDX22221	1621±92 (meas. in 2019)	398±92 (1σ)
	SG-OSL	crushed *terracotta* mortar	BDX22218	2139±162 (meas. in 2019)	-120±162 (1σ)
	SG-OSL	crushed *terracotta* mortar	BDX22219	2207±170 (meas. in 2019)	-188±170 (1σ)
Late Roman Antiquity wall, Gros-Pilier tower room, foundation wall 11109					
	^{14}C	charcoal	Lyon-14076(RICH)	1697±30 BP	[255; 286] (19%), [325; 418] (76%)
	SG-OSL	lime mortar	BDX22222	1648±162 (meas. in 2019)	371±162 (1σ)
	SG-OSL	lime mortar	BDX22223	1526±301 (meas. in 2019)	493±301 (1σ)
Late Roman Antiquity wall, section 11-300					
	Archaeomagnetism	brick	72181E_REN-2019-3	Inc=62.5° (63.2° at Paris), α_{95}=1.6°, k=226, N=35	[31; 157] (51%), [348; 456] (44%)
Excavation 11-600, mortar layer associated to the construction of the wall, us11607					
	^{14}C	charcoal	Lyon-17920(GrM)	1755±30 BP	[237; 401] (95%)
Excavation 11-600, layer us11625					
	Arch. artefact	*Crispus* coin			after 318-319
	Arch. artefact	Argonne ceramic			after 300
Before construction of the Late Roman Antiquity wall					
Early Empire structure, cellar of the city hall, wall 11120					
	^{14}C	charcoal	Lyon-15776(GrM)	1960±30 BP	[-40; 128] (95%)
	^{14}C	charcoal	Lyon-15777(GrM)	1975±30 BP	[-39; 121] (95%)
	^{14}C	charcoal	Lyon-15778(GrM)	1905±30 BP	[61; 217] (95%)
	^{14}C	charcoal	Lyon-15779(GrM)	1885±30 BP	[80; 99] (7%), [108; 234] (88%)
	SG-OSL	lime mortar	BDX22224	1780±161 (meas. in 2019)	239±161 (1σ)
	SG-OSL	lime mortar	BDX22225	1920±145 (meas. in 2019)	99±145 (1σ)
Early Empire structure, cellar of the city hall, wall 11107					
	^{14}C	charcoal	Lyon-14073(RICH)	1895±30 BP	[69; 225] (95%)
	SG-OSL	lime mortar	BDX22214	1800±114 (meas. in 2019)	219±114 (1σ)
	SG-OSL	lime mortar	BDX22215	1811±155 (meas. in 2019)	208±155 (1σ)
Excavation 11-600, Pit FS11648					
	^{14}C	charcoal	Lyon-17916(GrM)	2470±30 BP	[-764; -465] (93%), [-434; -421] (2%)
	^{14}C	charcoal	Lyon-17917(GrM)	2435±30 BP	[-748; -634] (29%), [-588; -406] (66%)
	^{14}C	charcoal	Lyon-17918(GrM)	2460±30 BP	[-755; -415] (95%)
	^{14}C	charcoal	Lyon-17919(GrM)	2460±30 BP	[-755; -415] (95%)

236

3. Laboratory methods

3.1 Radiocarbon

Most sampled charcoals (18/22) were included in mortar, others coming from the pit FS11648 in the excavation 11-600. Three bones were also dated, one included in the mortar of a medieval masonry and two from the burials SP11622 and SP11654 in the excavation 11-600. Almost all charcoals were first studied in anthracology by Aline Durand at the university of Le Mans. It highlights the predominant use of beeches and oaks in the production of the lime used in mortar making (Tab. S1 in supplementary material). Charcoals from young woods were preferentially selected for dating, in order to break free from old wood effect or at least minimize it. All the samples were prepared in Lyon. The charcoals were pre-treated by the classical acid-alkali-acid. The collagen of bones was extracted by the modified Longin method (Brown et al., 1988) after verification of its good preservation (Schoeninger et al., 1989) and assessment of the possible presence of carbon contamination (Drucker, 2001). Samples were then sent in the form of gas (CO_2) in sealed ampoules to Groningen (Netherlands) and Brussels (Belgium) laboratories where they were graphitized and measured by accelerator mass spectrometry (AMS). Conventional ^{14}C ages were calibrated with IntCal20 curve (Reimer et al., 2020).

3.2 Archaeomagnetism

Bricks acquired their thermoremanent magnetization (TRM) at the time of their last cooling from high temperature that is during their baking. Even if the precise location of the brick workshop(s) is unknown, the presence of exploitable clay deposits suggests that bricks were likely produced within 30 km from the city (Nauleau, 2021). For archaeomagnetic dating, we considered that the bricks were produced at Le Mans. Bricks were also baked in a different position than the one in the masonry, which means that only the archaeointensity of the geomagnetic field is theoretically preserved. However, in the case of parallelepipedal architectural baked clays as bricks, it is possible to recover the inclination under several hypothesis (Lanos, 1987, 1994). For the sake of

convenience and optimized storage inside the kiln, the first one is a disposition of the bricks on one of their planar sides during the baking, i.e. flat, upright or on the edge (Fig. 3a). On the assumption that the kiln floor was horizontal, the initial inclination is therefore preserved in one of these three positions. Only one provides an inclination value in agreement with the secular variation observed in France over the last millennia (50-75°, see e.g., Hervé and Lanos, 2018; Le Goff et al., 2020). It is therefore considered that the brick acquired its TRM in this position, making archaeomagnetic dating possible with the corresponding inclination value (Lanos, 1990). This approach also provides information on the arrangement of the bricks in the kiln (Lanos, 1994).

Here, the archaeomagnetic dating of the bricks from Le Mans Late Antiquity wall is based on the inclination. We could also study the archaeointensity but this parameter has a low chronological potential during the first half of the first millennium CE because the geomagnetic field strength did not vary significantly at this period in Western Europe (e.g., Gomez-Paccard et al., 2016; Rivero-Montero et al., 2021).

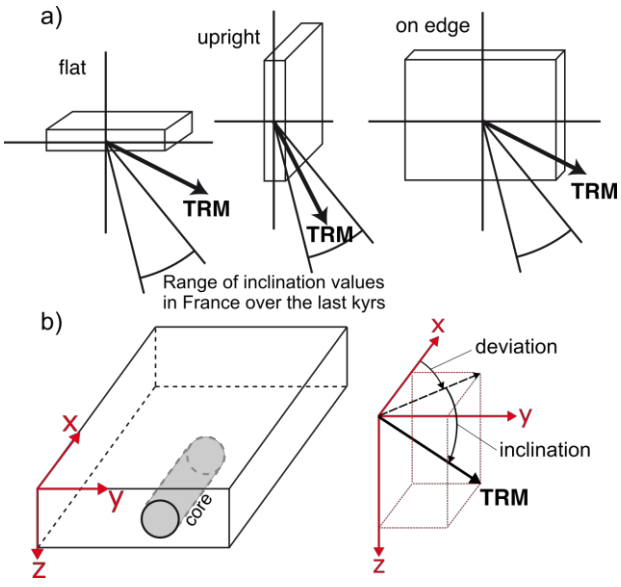

Figure 3: (a) In the hypothesis of a baking of the brick on one face, only one of the three possible positions provides an inclination value in agreement with the secular variation in France over the

last millennia (from Lanos, 1994). (b) Orientation of the archaeomagnetic specimens within the brick and directional components of the TRM in this coordinate system.

In order to take account for the uncertainties on the estimation of the inclination (for example the fact that bricks are not perfectly horizontal or vertical on the kiln floor), a large number of individual bricks, at least 50, is necessary (Lanos, 1994). The set of bricks must also appear homogeneous in terms of size and composition. The part of the Late Roman Antiquity wall that best met the criteria of number and homogeneity of bricks is the section 11-300 in the Pierre de Ronsard garden (Fig. 1d). Sampling focused on the lowest brick course, the best preserved, just above the large limestone blocks of the wall foundation and basement. 104 different bricks were sampled with 30, 49 and 25 bricks in the sections B, C and D respectively (Fig. S2a in supplementary material). The section A, visible over only a short length, was not studied. The extensive sampling allows to test the possibility of chronological differences between the bricks of the three sections and between the large (section C) and smaller (sections B+D) moduli, as well as the possibility of reuse of one of these subsets of bricks. In each brick, a core, one inch in diameter and 5-10 cm long, was drilled perpendicularly to the visible side using an electrically-powered device (Fig. S2b-c). After sampling, holes were finally filled by a self-made mortar of similar colour to the brick (Fig. S2d).

All experiments were performed at Rennes palaeomagnetic laboratory. First, cores were cut in 22-mm-long standard specimens (2 or 3 per core). Low-field susceptibilities were measured with a Bartington MS2 susceptibility meter and the remanent magnetizations with a Molspin spinner magnetometer. The direction of the magnetization was defined in a coordinate system relative to the brick (Fig. 3b). In this system, inclination is the angle between the TRM and the surface of the brick. The angle between the horizontal component of the TRM and the length of the bricks is called deviation. The direction of the TRM was determined after stepwise thermal demagnetization on one specimen per core. Specimens were heated in a MMTD80A furnace (Magnetic Measurements) with 8-9 steps between 100 and 525°C. The direction was calculated

by principal component analysis. In order to correct the TRM direction for anisotropy effect (e.g., Veitch et al., 1984), the TRM tensor of each specimen was estimated by six heating at 500°C in a laboratory field of 60 μT applied successively along +z, -z, +x, -x, +y and -y axes of the specimen (e.g., Chauvin et al., 2000). A last heating with the field along +z was finally performed to verify the absence of changes in the ferromagnetic mineralogy during the anisotropy protocol. The average inclination was calculated using McElhinny and McFadden (2000) statistics.

For dating, this average value was compared to the French secular variation curve recently updated by Le Goff et al. (2020). First, the inclination was recalculated from Le Mans to the reference location of the curve, Paris, using the assumption of a Geocentric Axial Dipole. The slight latitudinal difference (0.9°) between the two cities did not induce a significant relocation error. The dating process was performed on Chronomodel software (Lanos and Dufresne, 2019) with a prior period between 0 and 800 CE.

3.3 OSL

3.3.1 Some basics on OSL dating and types of studied samples

The well-known principle of OSL dating has been presented in numerous review articles (Aitken, 1998; Wintle and Murray, 2006). Let's recall that the OSL of minerals originates in the absorption of ionizing radiations coming from the natural radioactivity. In quantitative terms, the intensity of OSL signals is a function of the radiation dose absorbed by the dated material, since its zeroing process, the last light exposure or heating at more than 350°C. Like all paleo-dosimetric methods, the OSL age of a sample is given by the ratio of the average archaeological dose measured on the luminescent minerals selected for dating to the average annual dose rate to which these minerals were exposed during the archaeological times.

Here, OSL studies focused on the remains of the urban fortification in the cellars of the city hall and of the Gros-Pilier tower. Three types of materials were studied:

- Bricks: two samples taken from the gallery between the cellar and the lower room of the Gros-Pilier tower, belonging to the outer facade of the fortification (Fig. S1b).
- Lime mortar: Four samples were taken in the urban fortification itself, two from the foundation wall 11109 and two from the wall elevation 11108 (Fig. S1a-b). Four samples were also taken in the Early Empire walls 11107 and 11120 and two complementary in the wall 11121 of unknown period (Fig. S1c-d).
- Crushed *terracotta* mortar (*opus signinum*): this material consists in a lime mortar mixed with sand and millimetric fragments of tiles and bricks. Two samples were taken from the gallery close to the outer facade of the fortification by scrapping the surface of the masonry (Fig. S1d).

In the case of bricks, OSL dates their last heating, i.e., their production as archaeomagnetic dating does. In the case of lime mortars, the dated moment is the making of mortars, when lime and sand are mixed. Due to the forced movement of mixing, quartz grains from the sand are only shortly exposed to the ambient light when they reach the upper surface of the mixture and are thus bleached partially. In such conditions, the statistical distribution of light exposure of grains follows a decreasing exponential function (Guibert et al., 2017, 2020). In the case of crushed *terracotta* mortars, the interpretation of results depends on the origin of the quartz grains, either from the lime part or from the baked clay fragments. Apart from micro-dosimetric issues (hereafter reported), OSL dates theoretically the construction when the time lapse between the baked clay production and the making of mortar is unsignificant. Otherwise, the consideration of OSL signal of quartz grains from baked clay fragments provides a *terminus post quem* to the construction.

All samples were collected under very low intensity orange LED light and tightly packed in opaque boxes. The sample preparation is detailed in supplementary material.

3.3.2 Determination of annual dose

Concerning the determination of the dose rate components used in age calculation, different tools were used according to the origin of irradiation. The sample matrix contribution of brick or mortar was determined from low background gamma spectrometry measurements (Guibert et al., 2009b) that provided the K, U and Th contents of the material being dated, and the state of disequilibrium of the U-series. The K content was deduced from the single ^{40}K gamma line at 1460.8 keV. The Th content was determined by averaging all activities deduced from individual lines of ^{228}Ac, ^{212}Pb, ^{208}Tl and then was converted into mass concentration. In the U series, we distinguished different series of nuclides, that allowed us to evaluate the equilibrium state and thus the possible past changes of dose rate due to changes in radiochemical composition (more details for instance in Guibert et al., 2009b; Lahaye et al., 2012):

- the parent of the series given by ^{234}Th, ^{234m}Pa and ^{235}U emissions, the corresponding U content being denoted U(^{238}U);
- immediate daughters of ^{226}Ra given by ^{214}Pb and ^{214}Bi, the equivalent U content being denoted U(^{226}Ra), assuming equilibrium between ^{222}Rn and ^{226}Ra within the laboratory conditions;
- ^{210}Pb, the equivalent U concentration being denoted U(^{210}Pb).

The term “equivalent” illustrates the fact that the concentration of U was calculated from the corresponding isotopes, assuming secular equilibrium with their very first parents. Calibration uncertainties were around 1% for K, U(^{238}U), U(^{226}Ra), Th and 5% for U(^{210}Pb).

The elemental composition of samples was taken into account to correct intensities of gamma lines for the self-attenuation that affects gamma emissions and particularly the low energy ones like those of ^{210}Pb (46.5 keV) and ^{234}Th (63 keV). With these key-isotopes for the evaluation of the equilibrium state of U-series, the self-attenuation is dependent on the composition in major elements. In particular, this effect is important when comparing Ca rich samples, like mortars, to low Ca reference samples, like the granite GS-N used as a standard to determine the precise K, U and Th contents. All activities or mass contents of radio-elements were converted into the related dose rates using the conversion factors published by Guérin et al. (2011), accounting for possible

384 disequilibria in the U series (U/Ra variations and ^{222}Rn flux in sample, monitored by ^{210}Pb; see
385 Guibert et al., 2015 and Table S9 in supplementary material).
386 The environmental dose rate, which is the sum of gamma and cosmic dose rates, was measured at
387 the surface of every sampling location by on-site NaI:Tl gamma spectroscopy using a 1.5" × 1.5"
388 probe (the dimensions of the probe being around 5 cm in diameter and 12 cm in length, we
389 avoided to drill large holes in the masonry) designed to measure counts up to 10 MeV. The good
390 separation of the gamma spectral region (0-3 MeV) and the cosmic one (3-10 MeV) allowed to
391 differentiate easily the two dose components. On-site Al_2O_3:C dosimetry was also undertaken at a
392 10 cm depth inside the masonry at the precise location of the samples with pellets in a 12 mm
393 external diameter cylindrical container. This technique, less intrusive than gamma spectrometry,
394 integrates the whole environmental irradiation (gamma and cosmic rays). Finally, the
395 environmental dose rate of Le Mans samples was calculated as the mean value of on-site gamma
396 spectrometry and dosimetry, except for brick samples (BDX22220 and BDX22221) because only
397 NaI:Tl spectrometry data were available and for samples from the foundation wall 11109
398 (BDX22222 and BDX22223) for which the Al_2O_3 dosimetry results were preferred. In this latter
399 case, the presence of modern structures built close to the Late Roman Antiquity wall at this
400 location could have modified the "archaeological" gamma dose rate and we considered that the
401 dosimetry measurements inside the masonry were more significant than the spectrometry data
402 at the surface of the foundation wall.
403

404 **3.3.3 Determination of archaeological dose**

405 Standard OSL dating procedures were applied for dating bricks, following the usual single aliquot
406 regeneration (SAR) protocol on quartz inclusions (Murray and Wintle, 2000) according to the
407 classical multi-grain technique. In this study we used fine grains of quartz (3-11 μm) separated
408 from the powdered matrix using mechanical and chemical processes (Blain et al., 2007; see also
409 supplementary material). In addition to the usual determination of the archaeological dose by
410 beta laboratory irradiations, the alpha efficiency factor was measured using laboratory alpha

irradiations by a ^{241}Am source. We may note that the use of OSL is preferred to that of thermoluminescence (TL), since both OSL and TL can date the last heating of quartz minerals. The main reason is practical: the standard OSL protocol (SAR technique) is generally much more precise than the TL one ("added dose technique and regeneration after heating").

In the case of mortar samples, previous dating studies showed that it is necessary to examine the bleaching state of individual grains (e.g., Goedicke, 2003, 2011; Panzeri, 2013), especially for poorly bleached samples as we could expect here (Urbanová and Guibert 2017). A heterogeneous bleaching of quartz grains in the mortar results in an age overestimation with the multigrain technique. Therefore, all quartz grains, 200-250 μm in size, extracted from mortar samples (see supplementary material for the preparation of samples) were exclusively studied by the single grain technique, SG-OSL (Duller and Murray, 2000; Thomsen et al., 2005; Sim et al., 2013; Medialdea et al., 2014; Urbanová and Guibert, 2017). The OSL signal was measured grain by grain with a number of grains per sample between 2500 and 4000. Such high number of grains is necessary to analyse the dose distribution and obtain the significant chronological information carried by grains bleached during the mortar making. Specific tools are required to exploit the SG data and we used in this study the Exposure Exponential Distribution (EED) model, developed specifically for lime mortar dating (Guibert et al., 2017, 2020) (see supplementary material for details).

4. Results

4.1 Radiocarbon

Detailed ^{14}C results are presented in Table S1 in supplementary material and intervals of calibrated date at 95% of confidence in the Table 1. Dates from the same wall or structure are generally in agreement. The case of the first state of the masonry under the arcade is an exception with Lyon-15771(GrM) date on a small bone fragment is earlier than Lyon-15770(GrM) and Lyon-

15772(GrM) on charcoals. An older bone coming from the sand used in the mortar is the most likely explanation of this slight time shift.

The earliest structure is the pit FS11648 in the excavation 11-600, dated between ~750 and ~400 BCE in the Early Iron Age plateau of the calibration curve. Dates in the 1st and 2nd centuries CE on walls 11107 and 11120 confirm their attribution at the Early Empire period. The four dates associated to the Late Roman Antiquity fortification place its construction between ~240 and ~430 CE. Regarding the posterior structures, the two burials beneath the wall are not contemporaneous, one being dated ~600 CE and the other one on the 10th century. The dated walls around the collegiate are slightly later and concentrated between the second half of the 10th and the 12th century.

4.2 Archaeomagnetism

The intensities of the natural remanent magnetization (NRM) vary between 0.08 and 42 A/m and susceptibilities between 8×10^{-5} and 7×10^{-3} SI (Fig. S3 in supplementary material). Values are more grouped for bricks of larger modulus from section C. Bricks of smaller modulus from sections B and D have similar values that are well distributed all over the range of values. In archaeological baked clays, the variation of the NRM intensity and of the susceptibility mainly depends on the nature, size and number of ferromagnetic grains. These parameters are related to the firing conditions (temperature and redox conditions) and to the composition of the initial clay. The large variation of magnetic properties observed in the sections B and D might indicate the presence of several productions. However, we think that it is rather due to the variation of firing conditions inside the baking chamber of the kiln itself. Such variation is actually observed in experimental archaeology (e.g., Hervé et al., 2019).

The dominance of unblocking temperatures between 400 and 550°C given by thermal demagnetization suggest that the main carrier of the remanent magnetization is a titanium-poor titanomagnetite. Almost all specimens (97/104) present a single stable component of

462 magnetization after removing a slight component below 100-280°C that is likely of viscous origin
463 (Fig. 4a). The low-temperature component is larger, up to 360-420°C, in four bricks (Fig. 4b). In
464 such case, one can also assume that the brick moved during the cooling in the kiln. Finally, for 3
465 bricks from section C, the TRM does not pass through the origin of the orthogonal plot (Fig. 4c).
466 The temperature in these bricks was not high enough to erase previous remanent magnetizations.
467 This behaviour might be explained by a location of the brick on the edges of the kiln. The TRM
468 direction could be determined on 102/104 bricks and the TRM tensor calculated for 98 specimens
469 (see Tab. S2 in supplementary material). The value of the stability check of the anisotropy protocol
470 (%alt in Tab S2) is up to 5.2% and below 2.5% for 85% of specimens, highlighting the reliability
471 of the correction for the TRM anisotropy effect. Anisotropy degrees vary from 4 to 36% with
472 similar values between sections. The TRM anisotropy correction results in directional changes by
473 a few degrees.

474 In the brick coordinates system (i.e., as in Fig. 3b), the three possible positions during the baking,
475 flat, upright or on edge, correspond to a range of deviation and inclination values on a
476 stereographic plot (Fig. 4d). 93/98 bricks appear baked in the upright position, providing a
477 further example that this position largely prevailed at the Roman period (Lanos, 1994). For other
478 bricks, all from the section C, one was baked in the flat position and four on edge.

479 After rotation in the baking position, similar TRM directions are obtained in the three sections,
480 both in inclination and deviation (Figure 4e). They are distributed in two clusters of
481 complementary deviations, one centred around +10° and the other one around -80° (bricks with
482 deviations around +80–90° belong to this second group). This configuration, very common at the
483 Roman period, corresponds to a checkerboard positioning of the bricks inside a rectangular
484 cooling chamber (Lanos, 1990, 1994).

485 The relative scatter between inclination values requires investigation before to calculate the
486 average inclination. The method assumed that drilling was done in the flattening plane of the
487 brick. But it was not easy to core really perpendicular to the side of the brick and all bricks are not

exactly horizontal in the masonry, which results in random experimental errors. One can also notice a tendency of higher inclination values in the group with deviations around -80° than in the one with deviations around +10°. The effects of demagnetizing fields and of a dipping of the bricks could explain this difference (Lanos, 1994). The effect of demagnetizing fields, also named shape effect, occurs in flattened baked clays with a magnetization greater than 5–10 A/m (Lanos, 1987). For bricks baked upright, this effect results theoretically in an increase of the inclination (Lanos, 1990). Here, no differences of TRM inclination with NRM intensity are observed (Fig. S4 in supplementary material). Therefore, the difference in inclination between the two groups of deviations appears rather due to a slight dip (5-10° for example) of the bricks, a positioning that improves the stability of the loading in the kiln.

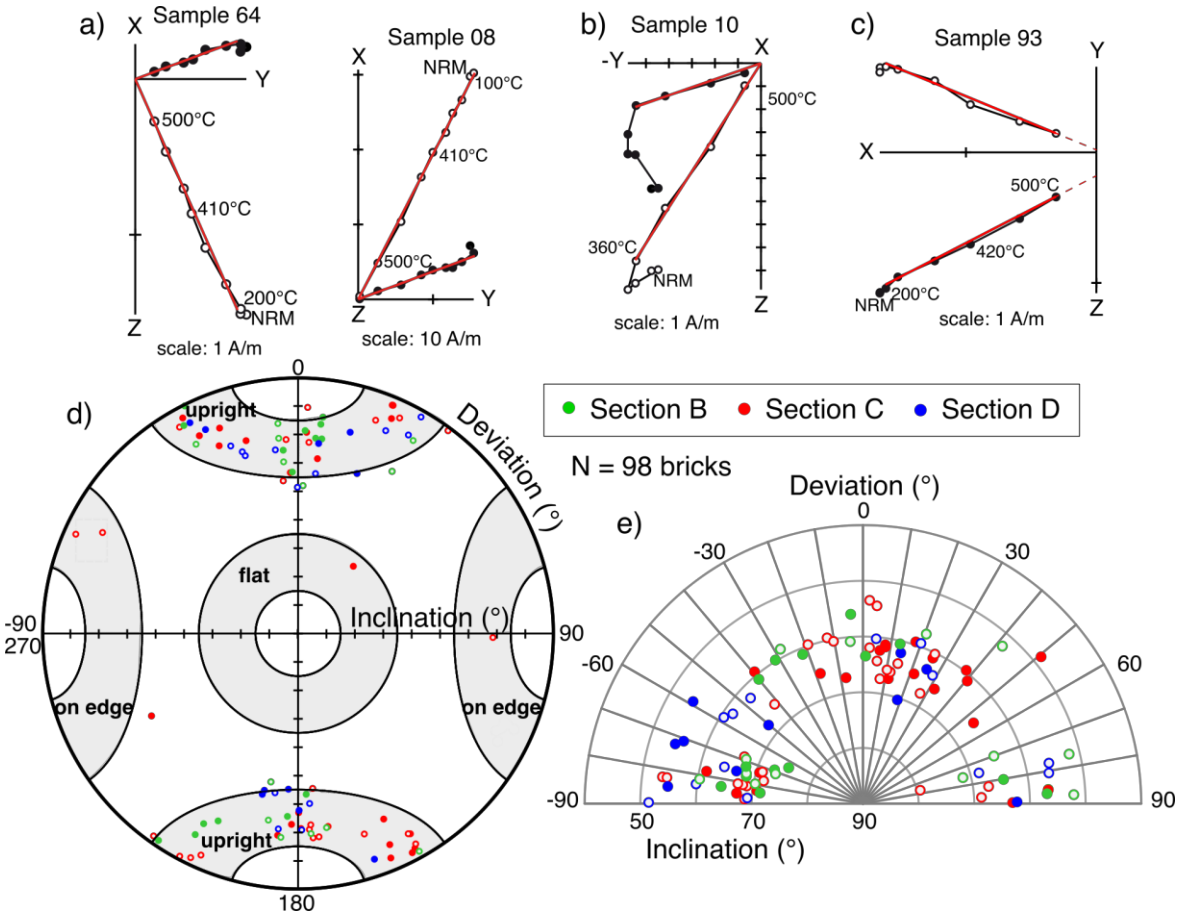

Figure 4: Archaeomagnetic directional results. (a-c) Representative orthogonal plots with open (solid) circles being the projections upon vertical (horizontal plane). The red line shows the direction of the TRM component determined by principal component analysis. (b) Stereographic

plot of TRM directions in the coordinate system of the brick after correction for TRM anisotropy. Solid and open circles correspond to positive and negative inclinations respectively. Grey shaded areas highlight range of values corresponding to the three possible positions in this coordinate system. (c) Stereographic plot of the directions after rotation in the baking position providing an inclination consistent with the secular variation (~55-75° in France).

Measurements on modern bricks and numerical simulations show that bricks with a deviation around 0°, i.e. with their flattening plane closely parallel to the surrounding geomagnetic field during the baking, preserved the true inclination value, while it is modified in bricks with deviation around 90° (Lanos, 1994). We consider thus that only the bricks with a deviation of +10±30°are relevant for the calculation of the average inclination. Among these 35 bricks, 5 come from the section B, 24 from the section C and 6 from the section D. The number of bricks per section is too low to be able to estimate a mean value for each of them. As inclinations are not significantly different between the three sections, the average value used for dating was calculated using the 35 selected bricks.

The average value of 62.5° has a radius of the 95% confidence circle (α_{95}) equal to 1.6° and a precision parameter (k) of 226. The comparison of the value relocated to Paris (63.2°) with the French secular variation curve (Le Goff et al., 2020) provides two intervals of date at 95% of confidence, [31; 157] and [348; 456] CE (Fig. 5). As the archaeological context favours the hypothesis of a production specifically for the construction of the section 11-300, archaeomagnetic dating indicates a baking of bricks more likely in the second interval between the middle of the 4th and the middle of the 5th century for. Nevertheless, archaeomagnetism alone cannot formally exclude that bricks were produced at the Early Empire period and reused from former buildings.

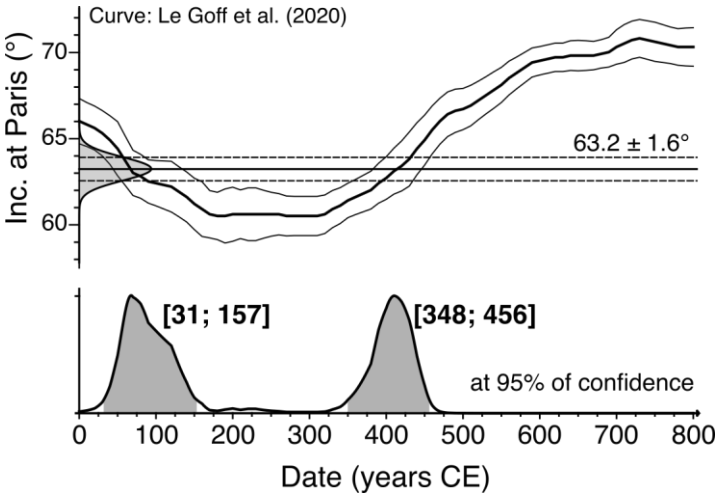

Figure 5: Archaeomagnetic dating of the bricks from section 11-300 of the Late Roman Antiquity wall. The comparison of the average inclination relocated to Paris provides a probability density function, on which are defined two intervals of date at 95% of confidence.

4.3 OSL

4.3.1 Determination of archaeological doses by OSL

SG OSL results for mortars are given in Table S3. The dose of individual grains ranged from 1 to more than 500 Gray (Gy) in lime mortar samples (Fig. 6). This large scatter, which is not abnormal with this type of sample, highlights a heterogeneous bleaching of the quartz grains. The concentration of grains in the low dose region corresponds to the best bleached grains. Conversely, the large tail towards high doses corresponds to unbleached or poorly bleached grains whose OSL shows the presence of residual "geological" signal characterizing the initial OSL state of the sedimentary sand used by the ancient masons. Only the mean archaeological dose corrected for these residuals is relevant to estimate the mean dose acquired by the studied quartz grains since the mortar making (see Guibert et al., 2020 for details).

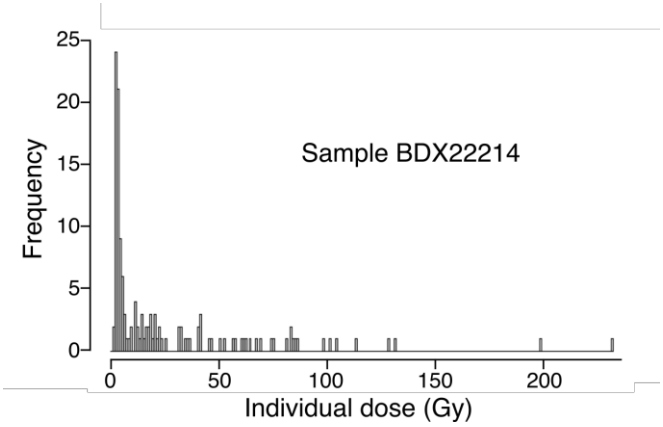

Figure 6: Histogram of individual equivalent doses of quartz grains extracted from a representative lime mortar sample (BDX22214).

The proportion of grains with a sufficiently intense OSL signal, i.e., usable for dose determination, is low, between 0.5 and 3.5 %, in lime mortars, while it reaches ~25-30% in crushed *terracotta* mortars (Tab. S5). In this type of mortar, as heating enhances the sensitivity to OSL, quartz grains from the baked clay fragments likely represents the most important part, ~90%, of grains with a measurable OSL signal. The higher representation of the baked clay fragments also results in kappa factors around 200 much higher than those of lime mortars. The low values of kappa in pure lime mortars, ranging between 2.6 and 7.8, indicate a relatively low level of exposure, corresponding approximately to a 5-15 seconds time of "full sun equivalent" mean exposure (Godfrey-Smith et al., 1988).

Finally, archaeological doses from standard OSL experiments on bricks are given in Tables S6 and S7. Bricks generally provide a more precise estimation than mortars, because the deposit of thousands of fine grains on discs results in a better reproducibility of OSL emissions compared to the SG-OSL results with a low number of measurable individual grains.

4.3.2 Determination of annual doses

The Table S8 reports the natural (i.e., as sampled) moisture content and radiochemical composition of the dried samples. The K-Th diagram illustrates important differences of internal radioactivity between bricks and mortars (Fig. 7). The crushed *terracotta* mortars exhibit a

radioactivity between bricks and pure lime mortars indicating a composition typically ca. 70% lime mortar and 30% crushed ceramic. These observations will help us to interpret the dating results on terracotta mortars in the next section.

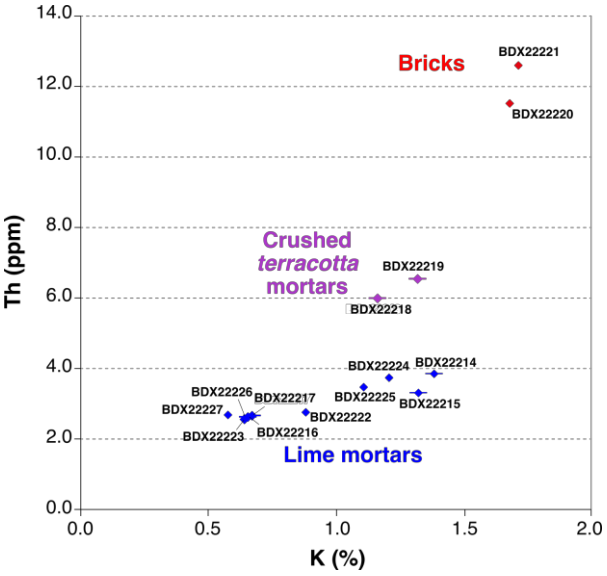

Figure 7: K-Th concentrations in OSL samples illustrating differences in internal radioactivity according to their nature.

A difference between uranium and radium activities can be observed in some samples (Tab. S8). This is related to the long-life elements that are potentially mobile due to weathering processes (Guibert et al. 2009b). A slight disequilibrium is observed in bricks and mortars, U(^{238}U) being lower than U(^{226}Ra), except for samples from the foundations of the Late Roman Antiquity wall (wall 11109) and from the Early Empire wall 11120. At the present stage of study, we cannot identify which element, U or Ra or even both, was affected by a variation of concentration in the past. The radon mobility (^{222}Rn), which is also a meaningful concern in luminescence dating, can be evaluated by comparing U(^{226}Ra) with U(^{210}Pb). As radiochemical analyses were performed shortly after sampling (i.e., some months), the activity of ^{210}Pb reflects the one of radon (^{222}Rn from ^{238}U series) during the last 30 years and thus characterizes the budget of radon within the materials under the archaeological conditions (before sampling and laboratory storage). In all samples, the absence of significant differences between ^{226}Ra and ^{210}Pb activities highlights no

588 transport of radon. Radium was likely a stable element at this site with no enrichment on grain
589 surfaces by precipitation from ground water. Otherwise, we would have observed a
590 disequilibrium with ^{210}Pb (less ^{210}Pb than ^{226}Ra), as the ^{222}Rn formed by decay of ^{226}Ra could not
591 have been maintained trapped inside minerals. According to this result, we consider that the
592 disequilibrium between ^{238}U and ^{226}Ra in almost all samples mainly originates in a movement of
593 uranium. The calculation of annual dose considers this disequilibrium, assuming it was constant
594 through time.
595 The Table S10 reports the different components of annual dose rates. Attenuation factors of alpha
596 and beta dose rates for the 200-250 µm quartz grains in mortars were deduced from Brennan et
597 al. (1991) and Mejdahl (1979) data. For these samples, the alpha efficiency factor was defined
598 with a standard value of k = 0.05±0.02 (Bailiff 2007, Guibert et al., 2009a), while the k-factor was
599 directly measured in the case of bricks studied using the quartz fine grain technique.
600
601 **4.3.3 Summary of OSL results**
602 The Table 2 reports archaeological doses, annual doses, OSL ages and dates, as well as their
603 statistical, systematic and total uncertainties. The total uncertainty is the quadratic sum of two
604 errors, the statistical one and the systematic one. The systematic uncertainty is related to the
605 calibration of measurements systems. For instance, the beta source calibration error for a given
606 OSL machine is a common uncertainty for all samples measured with that equipment.
607 The statistical uncertainty refers to the precision and the reproducibility of measurements within
608 a sample. The lowest values are observed on bricks mainly because the measurements with the
609 standard multigrain technique on quartz fine grains are very reproducible and because their k-
610 factor of the alpha efficiency is precisely measured. In mortar samples, the k-factor is a standard
611 value associated with a high uncertainty, although this disadvantage of SG-OSL technique is
612 minimized by the fact that the alpha annual dose is a very minor component because the
613 individual grains are around 10 times larger than the range of alpha particles. Apart these intrinsic
614 limitations, the higher statistical uncertainty of SG-OSL dates is also related to the dispersion of

615 the dose distribution and, further in our study, to the number of grains that are sufficiently bright
616 for dose measurement, the greater the number, the lower the statistical uncertainty.
617 The Late Roman Antiquity wall concentrates the most OSL results with 8 dates obtained on bricks,
618 lime mortars, crushed *terracotta* mortars from the wall itself (wall 11108) and on lime mortars
619 from its foundation (wall 11109). The SG-OSL dates (Tab. 2 and Fig. 8) on lime mortars are in
620 agreement within uncertainties between the walls 11108 and 11109 and centered on the Late
621 Roman Antiquity period (4-5th centuries). No significant gap is also observed with the results on
622 the two bricks. It suggests that bricks were produced for the construction and not reused from a
623 former monument but this hypothesis must be investigated with the whole set of dating results
624 (see section 5.1).
625 The two samples of crushed *terracotta* mortars provide earlier dates with an average in the
626 second century BCE. This apparent inconsistency with the archaeological context has a physical
627 explanation related to the different contributions of the lime mortar and baked clay fragments to
628 the archaeological and annual doses. The gamma spectrometry analysis indicates that these
629 samples are constituted by ca. 70% of pure lime and 30% of baked clay (Fig. 7) and the two
630 components take part to the annual dose in these proportions. However, in reason of their high
631 sensitivity (30% of grains with a sufficiently intense OSL signals, instead of 0.5-3.5% for unbaked
632 grains), grains from baked clay fragments represent around 90% of the accepted grains used for
633 the archaeological dose measurement. As a matter of fact, the proportion of the provenance of OSL
634 grains does not respect the proportion of materials (lime and baked clay). In addition, the
635 dimensions of the *terracotta* fragments (a few millimeters) imply that the beta dose-rate of the
636 dated grains originates essentially from the baked clay, much more radioactive than the major
637 component of the sample, the lime cement. As a result, the annual doses deduced from analyses
638 of the entire sample are underestimated and the corresponding ages are overestimated. However,
639 we can consider the OSL dates as *termini post quem* for the construction of the late Roman
640 Antiquity wall. Our results highlight that further research on OSL dating of crushed *terracotta*
641 mortars is required. Being able to separate the baked clay fragments from the rest of the mortar

642 would allow to better determine archaeological and annual doses, as well as to take into account
643 the probable use of "old" *terracotta*. Moreover, the high heterogeneity of the beta radiation field
644 within sample needs to be considered in the annual dose evaluation, by using for instance the
645 DOSIVOX facilities with complementary local elementary analysis of K, U and Th (Martin et al.,
646 2015).
647
648 Table 2: SG-OSL and OSL results. Location of the sample; laboratory name of the sample; type of
649 material; archaeological dose; annual dose; OSL age in years before the year of experiments
650 (2019); systematic uncertainty; statistical uncertainty; total uncertainty; date with 1σ standard
651 deviation. Uncertainties are expressed in standard deviation. Archaeological and annual dosses
652 are rounded to the second decimal.

Context	Sample	Material	Arch. dose (Gy)	Annual dose (mGy/yr)	Age (yrs)	Syst. unc. (yrs)	Stat. unc. (yrs)	Tot. unc. (yrs)	Date ± 1σ (yrs CE)
Late Roman Antiquity wall, gallery between the cellar of the city hall and the Gros-Pilier tower room, wall 11108									
	BDX 22216	lime mortar	1.56 ± 0.14	1.01 ± 0.06	1553	80	152	173	466 ± 173
	BDX 22217	lime mortar	1.49 ± 0.08	0.96 ± 0.05	1553	77	85	128	466 ± 128
	BDX 22220	brick	5.69 ± 0.26	3.23 ± 0.14	1762	86	50	107	257 ± 107
	BDX 22221	brick	5.35 ± 0.22	3.30 ± 0.15	1621	79	28	92	398 ± 92
	BDX 22218	crushed *terracotta* mortar	3.15 ± 0.02	1.47 ± 0.10	2139	120	106	162	TPQ :-120 ± 162
	BDX 22219	crushed *terracotta* mortar	3.45 ± 0.02	1.56 ± 0.11	2207	131	105	170	TPQ : -188 ± 170
Late Roman Antiquity wall, Gros-Pilier tower room, foundation wall 11109									
	BDX 22222	lime mortar	1.65 ± 0.12	1.00 ± 0.06	1648	99	127	162	371 ± 162
	BDX 22223	lime mortar	1.28 ± 0.21	0.84 ± 0.09	1526	91	286	301	493 ± 301
Early Empire structure, cellar of the city hall, wall 11120									
	BDX 22224	lime mortar	2.49 ± 0.17	1.40 ± 0.07	1780	99	127	161	239 ± 161
	BDX 22225	lime mortar	2.44 ± 0.10	1.27 ± 0.07	1920	107	96	145	99 ± 145
Early Empire structure, cellar of the city hall, wall 11107									
	BDX 22214	lime mortar	2.68 ± 0.08	1.49 ± 0.07	1800	92	63	114	219 ± 114
	BDX 22215	lime mortar	2.68 ± 0.18	1.48 ± 0.06	1811	92	124	155	208 ± 155
Undetermined period, cellar of the city hall, wall 11121									
	BDX 22226	lime mortar	2.55 ± 0.07	0.92 ± 0.05	2629	110	134	175	*-610 ± 175*
	BDX 22227	lime mortar	1.78± 0.12	0.89 ± 0.04	1973	101	147	179	*46 ± 179*

653
654
655 Regarding the former constructions, the OSL dates of the walls 11107 and 11120 are consistent
656 with each other and with stratigraphy. Conversely, the two OSL dates of the wall 11121, possibly
657 medieval, are problematic because of their large inconsistency and of their high ages. We have no

clear interpretation about such results. A hypothesis could be the fact that the mortar was prepared in very low light exposure conditions, for instance inside a pre-existing building (see Guibert et al., 2020 for a detailed discussion on this possible limitation of mortar dating by OSL). In such case, quartz grains could not be bleached at the mortar making and the OSL dates might be rather those of the sediment deposition (the sediment which was mixed with lime). Unfortunately, no charcoal could be found in the mortar of the wall 11121 in order to verify this hypothesis.

5. Discussion

5.1 Synthesis of chronological data

The results of all methods are plotted in Figure 8. Except the two burials, all structures have at least two dates with a maximum of 13 for the Late Roman Antiquity wall (including the two on crushed *terracotta* mortar). In the case of bricks, the two OSL dates confirm that the youngest date interval given by archaeomagnetism at the Roman period, i.e. [348; 456] CE, should be preferred. Overall, methods give consistent results for the Late Roman Antiquity wall, the Early Empire walls and medieval buildings. The wall 11121 in the cellar of the city hall constitutes the sole exception with a large disagreement between one OSL date at the turn of the Christian era and another one in the Early Iron Age, a period at which masonry was unknown in Northern Gaul. Our results cannot help to precise the date of construction, possibly medieval, of this wall.

All other chronological data were integrated in a hierarchical Bayesian model (Figure S5). We use Chronomodel 2.0 software (Lanos and Dufresne, 2019) that is based on the concept of Event date (Lanos & Philippe, 2018). An Event groups data coming from the same structure and therefore supposed contemporaneous. In addition to the experimental uncertainties, the Event model introduces an individual error on each data to take into account the possibility of a systematic error on the date. The relationships of anteriority or posteriority provided by the stratigraphy constitute prior information that helps to constrain the date of each event.

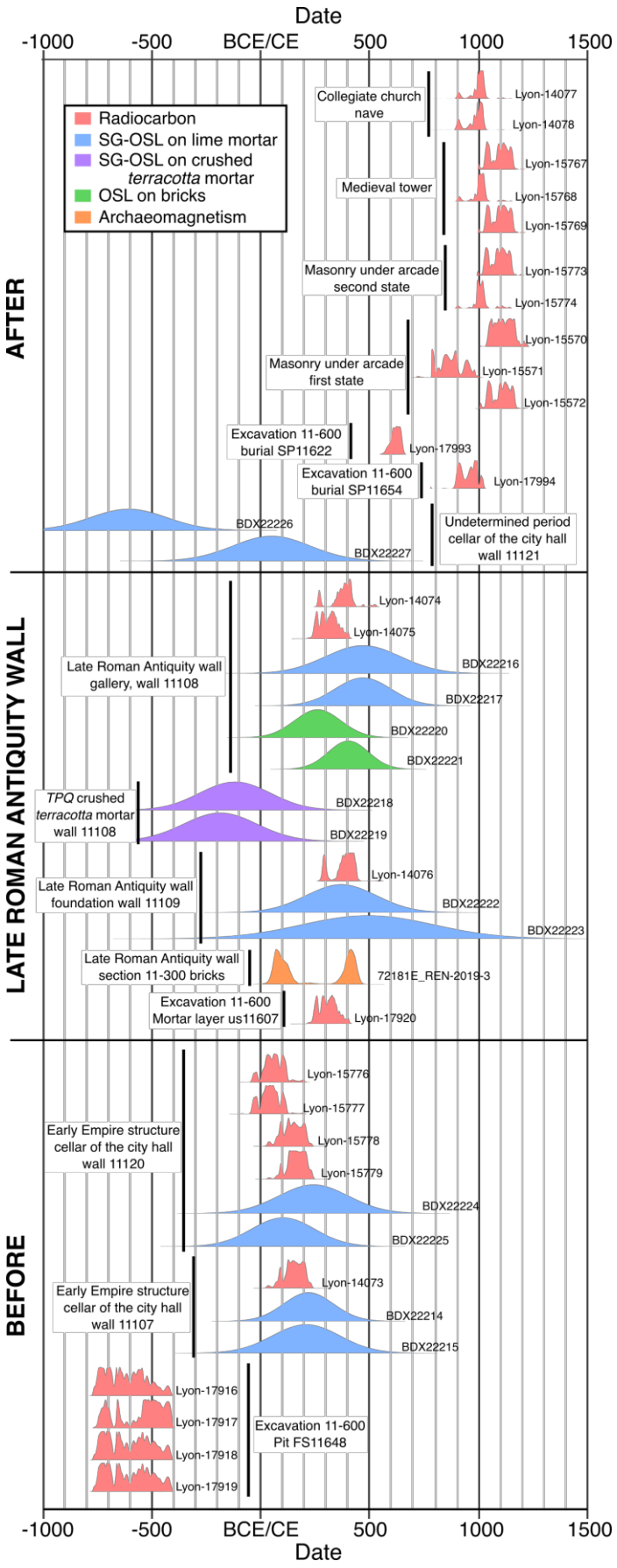

Figure 8: Summary of radiocarbon, SG-OSL, OSL and archaeomagnetic dates.

686

687 The main event of the model is related to the construction of the Late Roman Antiquity wall. We
688 decided to assign it all the radiocarbon, archaeomagnetic, OSL and SG-OSL dates on lime mortars
689 and bricks from the wall itself (wall 11108) and its foundations (wall 11109) (Figure S5). This
690 choice considers that studied bricks were not reused from a former monument but produced
691 specifically for the Late Roman Antiquity wall. In the sector 11, this hypothesis is supported by
692 the homogeneity of brick in sampled brick courses and not denied by the consistent results,
693 regarding experimental errors, on bricks and lime mortars. It is worth pointing out that this choice
694 could be not valid for another sector of the wall. Conversely, the two SG-OSL data on crushed
695 *terracotta* mortar are included in another event, because an intrinsic physical reason ascertain
696 that they do not date the construction but provide a *Terminus Post Quem*.

697 Besides physical dates, the model also integrates the dates of Crispus coin and Argonne *sigillata*
698 deposited shortly after the construction (see section 2.1), as well as those given by historical
699 sources and dendrochronology at the medieval period. These data, which constitute *Termini Post*
700 *Quem* or *Termini Ante Quem*, are not entered as events in Chronomodel but as bounds that are
701 defined as events with a known date.

702 The Bayesian model was performed with a prior study period between 1000 BCE and 1500 CE.
703 The Markov chain Monte Carlo (MCMC) process included 3 chains, each one with 100 k iterations
704 in the acquisition phase. Results of the model are presented in Figure 9 and discussed in the next
705 sections.

706

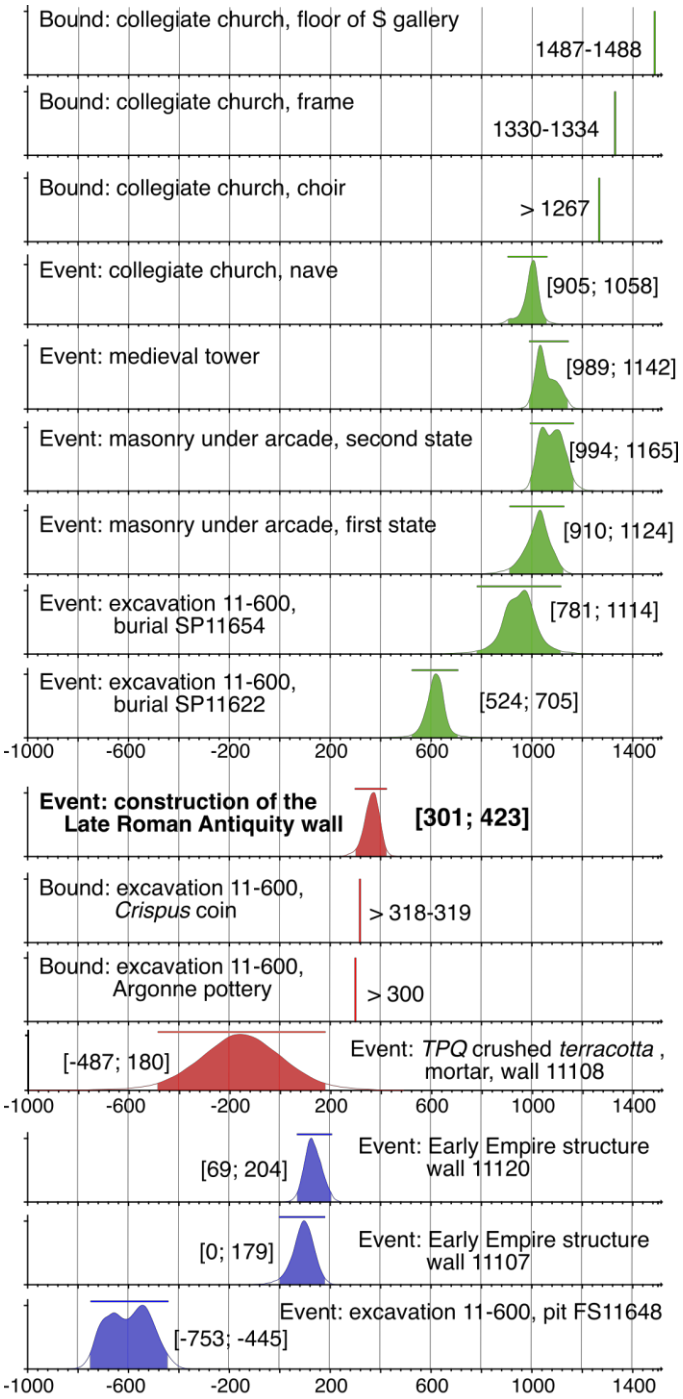

Figure 9: Results of Bayesian chronological modelling using Chronomodel 2.0 software with the probability density function (pdf) of each event. The line above the pdf indicates the highest posterior density intervals at 95% of confidence. The events and bounds related to the construction of the Late Antiquity Roman wall are in red, those before the construction in blue and those posterior to the construction in green.

714

715 **5.2 Construction of the Late Roman Antiquity urban fortification**

716 The Bayesian Event of the construction of the Late Roman Antiquity wall in the sector 11 presents
717 a monomodal probability density function providing an interval of date between 301 and 423 CE
718 at 95% of confidence. It is worth pointing out that this result does not depend on our choice to
719 include dates on lime mortars (radiocarbon and SG-OSL) and bricks (OSL and archaeomagnetism)
720 in the same event in the Bayesian model. Another model separating the two materials in two
721 different events give a very similar interval of date between 295 and 428 CE at 95% of confidence
722 for the building of the fortification.

723 The new dating invalidates the previous estimation of 280 ± 15 CE from Goulpeau (1985) given
724 by an archaeomagnetic study on a set of bricks from another sector of the wall in the western part
725 along the Sarthe River. Note that the unreliability of this previous date does not come from not
726 the result itself but from the dating process in use at this time. Using the statistically robust
727 modern Bayesian method, the average inclination (63.5 ± 3.0°, n=28 specimens, k=74) results in
728 an interval of [301; 551] at 95% of confidence, close to the values of the present new study.
729 Besides being more precise, our new date between 301 and 423 is also more reliable because it is
730 based on several methods and materials. The result is consistent with the *Termini Post Quem* of
731 the Crispus *nummus* coin and of the Chenet 320 cup in Argonne *sigillata* found in a layer shortly
732 deposited after the construction through excavation 11-600.

733 The new date between the beginning of the 4th century and the beginning of the 5th century clearly
734 excludes that the wall, at least in the studied sector, was built in the last third of the 3rd century as
735 previously thought. Therefore, the construction of the Late Roman Antiquity walls likely occurred
736 in a period characterized by a restoration of the imperial order and of economy, perhaps around
737 320-360 either under Constantine or one of his immediate successors. However, caution is needed
738 on this point because all new dates come from only one sector of the city, while the construction
739 of the overall urban fortification could last several decades.

Besides its chronological aspect, our study contributes to the knowledge of the construction work. In the sector of the Gros-Pilier tower, the dates obtained on the walls 11107 and 11120 ([0; 179] and [69; 204] CE at 95% of confidence respectively) show that the Late Roman Antiquity wall encompassed Early Empire walls. Moreover, if the large stone blocks from the foundation clearly came from former monuments of this period, the absence of a significant time shift between dates on bricks and lime mortars shows that, at least in this sector of the city, bricks were not reused from Early Empire constructions built before the mid 3rd century. Even though the dating uncertainties do not make impossible that they came from structures shortly built before, their size homogeneity within a section and the absence of fragmentation in the wall 11-300 strongly suggest that bricks were rather produced for the construction of the Late Roman Antiquity walls.

At the beginning of our study, the question of a reuse arose especially for the bricks of large modulus, as the size of bricks tended to decrease throughout the Roman period in Gaul (e.g., Nauleau, 2013). In the section 11-300, similar average inclination values are obtained for the bricks, having a 10±30° deviation, of small (61.8±2.7°, n=11 bricks) and large (62.8±1.9°, n=24 bricks) modulus. Therefore, the presence of two moduli likely corresponds to a procurement from at least two different workshops rather than by the reuse of one set of brick. Such multiple procurement is not surprising regarding the huge quantity (around 400,000) of bricks required for the construction of the urban walls (Nauleau, 2019).

Finally, the sector 11-300 divided in four different sections highlights the progressive construction of the fortification. The duration between the edification of each section was likely very short, from a few weeks to a few years, and the precision of dating techniques cannot be sufficient to investigate it.

5.3 Evolution of the sector 11 at the Medieval period

Our dating results clarify the chronology of the evolution of the Late Roman Antiquity walls in the sector 11 during the medieval period. First, recent archaeological excavations, as in the 11-600

766 area, highlight the presence of burials against the base of the wall (Bouillet et al., 2022). The two
767 radiocarbon dates circa 600 CE for the burial SP11622 ([574; 651] Cal yrs CE at 95% of
768 confidence) and in the 10th century for the burial SP11654 ([891; 996] and [1003; 1020] Cal yrs
769 CE at 95% of confidence) show that this practice lasted over all the Early Middle Age.

770 At the same period, important civil buildings, which became later the Counts of Maine residence
771 at the present location of the city hall and collegiate church Saint-Pierre-de-la-Cour, were
772 probably built within the city walls against the fortification. However, the architecture of the walls
773 themselves does not seem significantly modified in this sector before the 10-11th centuries and
774 the construction of the first collegiate church.

775

776 **6. Conclusion**

777 Based on 40 new ^{14}C, OSL (quartz fine grain technique), SG-OSL and archaeomagnetic dates in a
778 limited well-preserved sector, our study reassesses the date of construction of the Late Roman
779 Antiquity walls and precises the evolution of this area from the protohistoric to the medieval
780 periods. All results were integrated in a Bayesian chronological model together with stratigraphy
781 and temporal constraints provided by archaeological artefacts and historical sources. The
782 chronological model dates the construction of the Late Roman Antiquity walls between 301 and
783 423 CE at 95% of confidence. This result unambiguously excludes that it occurred during the
784 crises of the 3rd century, as previously thought, but rather in the stable political context of the 4th
785 century.

786 Besides chronological aspects, crossing dating methods give information on the construction
787 work of the Late Roman Antiquity walls. The consistency of archaeomagnetic and OSL dates on
788 bricks with the ^{14}C and SG-OSL dates on lime mortars shows that bricks were not reused from
789 former building, at least in this sector of the walls. They were produced for the construction of the
790 walls with the presence of several types of bricks likely reflecting a supply from at least two local
791 workshops.

From a methodological point of view, this study constitutes a new example of the applicability of SG-OSL to date lime mortars. Conversely, further methodological research is required for crushed *terracotta* mortars. For physical reasons, their mixed composition of lime mortar and baked clay fragments can only provide a *Terminus Post Quem* to the construction.

Finally, our study shows the importance of crossing dating methods in a close interdisciplinary collaboration to get the most relevant information. The use of a single dating method (OSL or radiocarbon or archaeomagnetism) would not have allowed such robust chronology and interpretations of the building of the Late Roman Antiquity walls, because each method dates different events (manufacture of bricks by archaeomagnetism and OSL, growth of vegetal elements corresponding to the charcoals embedded in mortar by ^{14}C, making of mortar by SG-OSL). Crossing all these chronological events is then much more suitable for the knowledge of the construction. In addition, typochronological methods can admittedly be more precise but artefacts clearly associated to the building are very rare, or even exceptional (i.e., accidental?), in such archaeological contexts. The *Crispus* coin and the Argonne ceramic found in the excavation 11-600 were in fact unexpected at the starting of the study. The good results of our methodology encourage its application in other Late Roman Antiquity fortifications. Revisiting their chronology would help to better understand the historical context of the development of these monumental constructions.

Acknowledgements

This study was supported by the *Projet Collectif de Recherche* on the Late Roman Antiquity wall of Le Mans, directed by two of us (Hugo Meunier and Martial Monteil). We warmly acknowledge the funders of this program, the Regional Direction of Cultural Affairs (*DRAC – Service regional de l'archéologie*) of the region Pays-de-la-Loire and the city of Le Mans. This research has also benefited from the contributions of CNRS-INSHS (French National Centre for Scientific Research - Institute of Human and Social Sciences) [salary], University Bordeaux-Montaigne [Master grant and special support for research programs], University of Bordeaux ["chaire junior" program].

The OSL dating equipment used in this study was formerly funded by the Regional Council of Aquitaine, the University Bordeaux Montaigne, the CNRS, and by the labex LaScArBx [Bordeaux Archaeological Sciences Labex] administrated by ANR [Agence Nationale de la Recherche] with the reference ANR-10-LABX-52. We are grateful to Gérard Aubin (Inspecteur general honoraire de l'archéologie) for the study of coins, Aline Durand (Le Mans Université, UMR 6566 CReAAH) for her anthracological analyses of charcoals before dating, Christian Le Boulaire (Direction du patrimoine et de l'archéologie de Nantes métropole, UMR 6566 CReAAH-LARA) for the study of pottery artefacts and Jean-François Nauleau for the morphometric analysis of studied bricks. Finally, we acknowledge three anonymous reviewers for their comments and Dr. Ellery Frahm for editorial handling.

References

Aitken, M. J., 1998. An Introduction to Optical Dating. The Dating of Quaternary Sediments by the Use of Photon Stimulated Luminescence. Oxford Science Publications, Oxford.

Bailiff, I. K., 2007. Methodological developments in the luminescence dating of brick from English late-medieval and post-medieval buildings. Archaeometry, 49, 827-851. http://dx.doi.org/10.1111/j.1475-754.2007.00338.x.

Bailiff, I. K., Holland, N., 2000. Dating bricks of the two last millennia from Newcastle upon Tyne: a preliminary study, Radiation Measurements, 32, 615- 619.

Bayard, D., Fourdrin, J.-P. (eds), 2019. *Villes et fortifications de l'Antiquité tardive dans le Nord de la Gaule, Actes du colloque de Villeneuve d'Ascq et Bavay, 25-27 mars 2015*, Lille, Revue du Nord (hors-série, coll. Art et Archéologie, 26), 451 p.

Blain, S., Guibert, P., Bouvier, A., Vieillevigne, E., Bechtel, F., Sapin, C., Baylé, M., 2007, TL-dating applied to building archaeology: The case of the medieval church Notre-Dame-Sous-Terre (Mont-Saint-Michel, France), Radiation Measurements, 42, 1483-1491.

Bocquet, A., Meunier, H., Monteil, M., Mortreau, M., Sarreste, F., 2022., Villes et campagnes des cités des Aulerques Cénomans et Diablintes entre les III^e et VII^e s. apr. J.-C., *In* Chambon, M.-P., Crogiez-Pétrequin, S., Ferdière, A., Janniard, S. (eds.), *L'Antiquité tardive dans le centre et le centre-ouest de la Gaule (III^e-VII^e siècles)*, *Actes du colloque international ATEG VI, Tours, 6-8 décembre 2018, Tours*, FERACF (coll. Supplément. à la *Revue archéologique du Centre de la France*, 81), 167-187.

Bouillet, J., Augry, S., Bertrand, E., Meunier, H., Monteil, M. (eds.), 2022. Au pied du mur, l'enceinte romaine du Mans. Catalogue de l'exposition du musée Jean-Claude Boulard – Carré Plantagenêt, Le Mans, Musées du Mans, Ed. Snoeck, Gand, 200 pp.

Brennan, B. J., Lyons, R. G., Phillips S.W., 1991. Attenuation of alpha particle track dose for spherical grains. International Journal of Radiation Applications and Instrumentation. Part D. Nuclear Tracks and Radiation Measurements 18: 249–253.

Bronk Ramsey, C., 2009. Bayesian Analysis of Radiocarbon Dates, Radiocarbon, 51, 1, 337-360.

Brown, M. C., Hervé, G., Korte, M., Genevey, A., 2021. Global archaeomagnetic data: The state of the art and future challenges. Phys. Earth Planet. Inter., 318, 106766.

Brown, T.A., Nelson, D.E., Vogel, J. S., Southon, J. R., 1988. Improved collagen extraction by modified Longin method. Radiocarbon, 30(2), 171-177.

Buck, C.E., Millard, A. R. (eds), 2004, *Tools for Constructing Chronologies, Crossing Disciplinary Boundaries*, Series : Lecture Notes in Statistics, 177, Springer-Verlag, Londres, 2004.

Chauvin, A., Garcia, Y., Lanos, P., Laubenheimer, F., 2000. Paleointensity of the geomagnetic field recovered on archaeomagnetic sites from France. Phys. Earth Planet. Inter. 120, 111–136.

De Fillippo, R., 2004. La brique et les matériaux de construction en terre cuite à l'époque romaine. In La construction: les matériaux durs, pierre et terre cuite. (J.-C. Bessac, O. Chapelot, R. De Fillippo, eds), 97-116, Paris, Errance.

Drucker, D., 2001. Validation méthodologique de l'analyse isotopique d'ossements fossiles et apports aux reconstitutions paléoécologiques du Paléolithique supérieur du sud-ouest de la France, thèse de doctorat de l'Université de Pierre et Marie Curie, Paris.

Duller, G., Murray, A.S., 2000. Luminescence dating of sediments using individual mineral grains. Andean Geol. 5, 87–106.

Fourdrin, J.-P. (ed.), 2020. *Les Enceintes urbaines de Novempopulanie entre Aquitaines et Hispanies, Actes du colloque international, Pau, Université de Pau et des pays de l'Adour, 4-5 novembre 2011*, Pau, Presses de l'Université de Pau et des pays de l'Adour (coll. *Archaia*, IV), 2020, 280 pp.

Gallet, Y., Genevey, A., Le Goff, M., Warmé, N., Gran-Aymerich, J., Lefèvre, A., 2009. On the use of archaeology in geomagnetism, and vice-versa: recent developments in archeomagnetism, *C.R. Physique*, 10**,** 630–648, doi:10.1016/j.crhy.2009.08.005.

Godfrey-Smith, D., I., Huntley, D., J., Chen, W., H., 1988. Optical dating studies of quartz and feldspar sediment extracts. Quaternary Science Reviews, 7, 373–380.

Goedicke C, 2003. Dating historical calcite mortar by blue OSL: results from known age samples. Radiation Measurements 37: 409–415, doi:10.1016/S1350-4487(03)00010-6.

Goedicke, C., 2011. Dating mortar by optically stimulated luminescence: a feasibility study. Geochron., 38, 1, 42-49.

Gómez-Paccard, M., Osete, M.L., Chauvin, A., Pavón-Carrasco, F.J., Perez-Asensio, M., Jimenez, P., Lanos, P., 2016. New constraints on the most significant paleointensity change in Western Europe over the last two millennia. A non-dipolar origin? Earth planet. Sci. Lett. 454, 55–64.

Goulpeau, L., 1985. Compte-rendu de l'étude archéomagnétique de la datation des structures du site de Le Mans, enceinte gallo-romaine. Report. University of Rennes, 4 p.

Guérin, G., Mercier, N., Adamiec, G., 2011. Dose-rate conversion factors: update. Ancient TL, 29, 5-8.

Guibert, P., Urbanová, P., 2022. Recherches en chronologie : Archéologie du bâti et méthodes de datation, usages et potentialités en 2020. In Archéologie du bâti. Aujourd'hui et demain (eds C. Sapin, S. Bully, M. Bizri, F. Henrion), 25 pp. ARTEHIS Editions, Dijon. Available at http://books.openedition.org/artehis/27212

Guibert, P., Bailiff, I. K., Blain, S., Gueli, A., Martini, M., Sibilia, E., Stella, G., Troja, S., 2009a. Luminescence dating of architectural ceramics from an early medieval abbey: the St-Philbert intercomparison (Loire Atlantique, France). Radiation Measurements 44: 488–493, doi:10.1016/j.radmeas.2009.06.006.

Guibert, P., Lahaye, C., Bechtel, F., 2009b. The importance of U-series disequilibrium of sediments in luminescence dating: a case study at the Roc de Marsal cave (Dordogne, France), Radiation Measurements, 44, 223-231.

Guibert, P., Bailiff, I. K., Baylé, M., Blain, S., Bouvier, A., Büttner, S., Chauvin, A., Dufresne, P., Gueli, A., Lanos, P., Martini, M., Prigent, D., Sapin, C., Sibilia, E., Stella, G., Troja, O., 2012. The use of dating methods for the study of building materials and constructions: state of the art and current challenges. In Carvais, R., Guillerme, A., Nègre, V., Sakarovitch, J. (eds), Proceedings of the 4th International Congress on Construction History, Paris 3-7 July 2012, Nuts and Bolts of Construction History, Culture, Technology and Society, Vol. 2, Ed. Picard, 469-480.

Guibert P., Brodard A., Quilès A., Geneste J.-M., Baffier D., Debard E., Ferrier C., 2015. When were the walls of the Chauvet Pont-d'Arc Cave heated? A chronological approach by thermoluminescence. Quaternary Geochronology, 29, 36-47. doi:10.1016/j.quageo.2015.04.007

Guibert, P., Christophe, C., Urbanová, P., Blain, S., Guérin, G. 2017. Modeling incomplete and heterogeneous bleaching of mobile grains partially exposed to the light: towards a new tool for single grain OSL dating of poorly bleached mortars, Radiation Measurements, 107, 48-57.

916 Guibert, P., Urbanová, P., Javel, J.-B., Guérin, G., 2020. Modelling light exposure of quartz grains
917 during mortar making: consequences for optically stimulated luminescence dating. Radiocarbon,
918 62, 3, 693-711.

919 Guilleux, J., 2000. *L'Enceinte romaine du Mans,* Saint-Jean-d'Angély, J.-M. Bordessoules, 2000, 268
920 p.

921 Hervé G. & Lanos, P., 2018. An alternative to the problem of the Hallstattian plateau effect:
922 Improvements of archaeomagnetic dating in Western Europe from the Late Bronze to the Late
923 Iron Ages. Archaeometry 40, 870-883.

924 Hervé, G., Chauvin, A., Lanos, P., Rochette, P., Perrin, M., Perron d'Arc, M., 2019. Cooling rate effect
925 on thermoremanent magnetization in archaeological baked clays: an experimental study on
926 modern bricks. Geophys. J. Int. 217 (2), 1413–1424.

927 Intagliata, E., Barker, S. J., Courault, C., 2020. *City walls in Late Antiquity. An empire-wide*
928 *perspective*, Oxford, Philadelphie, Oxbow books, 2020, 174 p.

929 Lahaye, C., Guibert, P., Bechtel, F., 2012, Uranium series disequilibrium detection and annual dose
930 determination: A case study on Magdalenian ferruginous heated sandstones (La Honteyre,
931 France), Radiation Measurements, 47, 786-789. doi:10.1016/j.radmeas.2012.02.002

932 Lanos, 1987. The effects of demagnetizing fields on thermoremanent magnetization avquired by
933 parallel sided baked clay blocks. Geophys. J. Int. 91(3), 985-1012.

934 Lanos, P., 1990. La datation archéomagnétique des matériaux de construction d'argile cuite.
935 Apports chronologiques et technologiques. Gallia, 47, 321-341.

936 Lanos, P., 1994. Pratiques artisanales des briquetiers et archéomagnétisme des matériaux d'argile
937 cuite: Une histoire de positions de cuisson. Histoire *& Mesure*, 9(3-4), 287-304.

938 Lanos, P., 2004, Bayesian inference of calibration curves: application to archaeomagnetism, in
939 Tools for constructing chronologies: crossing disciplinary boundaries (eds. C. E. Buck and A. R.
940 Millard), 43–82, Springer, London.

941 Lanos P., Dufresne P., 2012. Modélisation statistique bayésienne des données chronologiques, *in*
942 Beaune (de), S.A., Francfort, H.-P. (eds), *L'archéologie à découvert*, éd. CNRS Editions, Paris, 238-
943 248.

944 Lanos, P., Dufresne, P., 2019. ChronoModel version 2.0: Software for Chronological Modelling of
945 Archaeological Data using Bayesian Statistics. Available at https://chronomodel.com/

946 Lanos, P., Philippe, A., 2018. Event date model: a robust Bayesian tool for chronology building.
947 Commun. Stat. Appl. Methods 25, 131e157. https://doi.org/10.29220/ CSAM.2018.25.2.131.

948 Lanos, P., Dufresne, P., Garnier, L., 2015. *Le Mans (Sarthe). Enceinte gallo-romaine. Lot de briques*,
949 Rapport d'analyse archéométrique, Rennes, IRAMA-CRPAA, 12 pp.

950 Le Goff, M., Gallet, Y., Warmé, N., Genevey, A., 2020. An updated archeomagnetic directional
951 variation curve for France over the past two millennia, following 25 years of additional data
952 acquisition. Phys. Earth Planet. Inter. 309, 106592.

953 Martin, L., Mercier, N., Incerti, S., 2015. DosiVox: Implementing Geant 4-based software for
954 dosimetry simulations relevant to luminescence and ESR dating techniques. Ancient TL, 33, 1, 1-
955 10.

956 McElhinny, M. W. & McFadden, P. L., 2000. *Paleomagnetism: continents and oceans.* International
957 Geophysics Series, 73, Academic Press, San Diego.

958 Medialdea, A., Thomsen, K. J., Murray A. S., Benito G., 2014. Reliability of equivalent-dose
959 determination and age-models in the OSL da-ting of historical and modern palaeoflood sediments.
960 Radiation Measurements 22: 11–24, doi:10.1016/j.quageo.2014.01.004.

961 Mejdahl, V., 1979. Thermoluminescence dating: beta-dose attenuation in quartz grains.
962 Archaeometry 21: 61–72, doi:10.1111/j.1475-4754.1979.tb00241.x.

963 Meunier, H., Augry, S., 2019. L'enceinte romaine du Mans et ses abords : synthèse des dernières
964 interventions archéologiques, *in* Bayard, D., Fourdrin, J.-P. (eds), *Villes et fortifications de*

l'Antiquité tardive dans le Nord de la Gaule, Actes du colloque de Villeneuve d'Ascq et Bavay, 25-27 mars 2015, Lille, Revue du Nord (hors-série, coll. Art et Archéologie, 26), 293-314.

Meunier, H., Monteil, M., 2019a. Le Mans. L'enceinte romaine et la nef de la collégiale comtale Saint-Pierre-de-la-Cour, *Bulletin monumental*, 177-1, 59-63.

Meunier, H., Monteil, M. (eds.), 2019b. *Projet collectif de recherche, L'enceinte romaine du Mans (Sarthe, Pays de la Loire). Bilan des connaissances,* Rapport d'activités 2018, Nantes, Archives scientifiques du Service Régional de l'Archéologie des Pays de la Loire, 246 pp.

Meunier, H., Monteil, M. (eds.), 2020. *Projet collectif de recherche, L'enceinte romaine du Mans (Sarthe, Pays de la Loire). Bilan des connaissances,* Rapport d'activités 2019, Nantes, Archives scientifiques du Service Régional de l'Archéologie des Pays de la Loire, 432 pp.

Meunier, H., Monteil, M. (eds.), 2021. *Projet collectif de recherche, L'enceinte romaine du Mans (Sarthe, Pays de la Loire). Bilan des connaissances,* Rapport d'activités 2020, Nantes, Archives scientifiques du Service Régional de l'Archéologie des Pays de la Loire, 339 pp.

Meunier, H., Monteil, M., Augry, S., 2022. L'enceinte romaine du Mans : une construction monumentale, in *L'enceinte romaine du Mans. 40 ans de recherche archéologique*, Dijon, Éditions Faton (coll. *Archéologia*, hors-série 34), p. 22-35.

Murray, A.S., Wintle, A., 2000. Luminescence dating of quartz using an improved single-aliquot regenerative dose protocol. Radiation Measurements, 32, 523–538.

Nauleau, J.-F., 2013. Les matériaux de construction en terre cuite d'époque romaine dans l'ouest des Pays de la Loire – Premier bilan. Revue Archéologique de l'Ouest, 30, 223-259.

Nauleau, J.-F., 2019. Les matériaux de construction: les terres cuites architecturales. In Monteil, M., Meunier, H. (eds). L'enceinte romaine du Mans, bilan des connaissances, Projet collectif de recherche 2018-2020, Rapport d'activités 2018, Nantes, Archives scientifiques du Service Régional de l'Archéologie des Pays de la Loire, 201-209.

Nauleau, J.F., 2021. Contribution à l'étude de provenance des matériaux en terre cuite à partir de la localization des tuileries médiévales, modernes et contemporaines. In Monteil, M., Meunier, H. (eds). L'enceinte romaine du Mans, bilan des connaissances, Projet collectif de recherche 2018-2020, Rapport d'activités 2020, Nantes, Archives scientifiques du Service Régional de l'Archéologie des Pays de la Loire, 283-298.

Panzeri, L., 2013. Mortar and surface dating with optically stimulated luminescence (OSL): innovative techniques for the age determination of buildings. Nuovo Cimento della 36 (4), 205–216.

Panzeri, L., Caroselli, M., Galli, A, Lugli, S., Martini, M., Sibilia, E., 2019. Mortar OSL and brick TL dating: the case study of the UNESCO World Heritage Site of Modena, *Quaternary Geochronology*, 49, 236-241.

Panzeri, L., Maspero, F., Galli, A., Sibilia, E., Martini, M., 2020. Luminescence and Radiocarbon Dating of mortars at Milano-Bicocca laboratories, *Radiocarbon*, Vol 62, 657-666.

Pithon, M. (coord.), Bocquet, A., Comte, F., Favreau, X., Laurens-Berge, M., Le Boulaire, C., Mercier, F., Meunier, H., Monteil, M., Mortreau, M. avec la collab. de Jarousseau, G., 2022. Angers, Jublains, Le Mans et Nantes. Quatre chefs-lieux de cité antiques à l'époque mérovingienne. État des connaissances, *in* Henigfeld, Y., Peytremann, É. (eds), *Un monde en mouvement. La circulation des hommes, des biens et des idées à l'époque mérovingienne (V^e^-VIII^e^ siècle), Actes des 40^e^ journées internationale de l'Association française d'archéologie mérovingienne, Nantes, 3-5 octobre 2019*, Saint-Germain-en-Laye, AFAM (coll. Mémoires de l'AFAM, 37), p. 337-359.

Reimer, P., Austin, W., Bard, E., Bayliss, A., Blackwell, P., Ramsey, C., Butzin, M., Cheng, H., Edwards, R., Friedrich, M., Grootes, P., Guilderson, T., Hajdas, I., Heaton, T., Hogg, A., Hughen, K., Kromer, B., Manning, S., Muscheler, R., Palmer, J., Pearson, C., van der Plicht, J., Reimer, R., Richards, D., Scott, E., Southon, J., Turney, C., Wacker, L., Adolphi, F., Büntgen, U., Capano, M., Fahrni, S., Fogtmann-Schulz, A., Friedrich, R., Köhler, P., Kudsk, S., Miyake, F., Olsen, J., Reinig, F., Sakamoto, M., Sookdeo,

A., Talamo, S., 2020. The IntCal20 Northern Hemisphere radiocarbon age calibration curve (0-55 Cal kBP). Radiocarbon 62, 725–757. https://doi.org/10.1017/RDC.2020.41.

Rivero-Montero, M., Gómez-Paccard, M., Pavón-Carrasco, F.J., Cau-Ontiveros, M.A., Fantuzzi, L., Martin-Hernandez, F., Palencia-Ortas, A., Aidona, E., Tema, E., Kondopoulou, D., Mas-Florit, C., Ramon-Torres, J. 2021. Refining geomagnetic field intensity changes in Europe between 200CE and 1800 CE. New data from the Mediterranean region. Phys. Earth Planet. Inter., 317, 106749.

Schoeninger, M.J., Moore, K. M., Murray, M.L., Kingston, J.D., 1989. Detection of bone preservation in archaeological and fossil samples. Applied Geochemistry, 4, 281-292.

Sim, A. K., Thomsen, K. J., Murray, A. S., Jacobsen, G., Drysdale, R., Erskine, W., 2013. Dating recent floodplain sediments in the Hawkesbury-Nepean River system using single grain quartz OSL. Boreas 43(1): 1–21, doi:10.1111/bor.12018.

Sotinel, C. Virlouvet, C. (eds.), 2019. *Rome, la fin d'un empire. De Caracalla à Théodoric, 212 – fin du v^e^ siècle*, Paris, Belin (coll. Mondes anciens), 688 p.

Stella, G., Fontana, D., Gueli, A.M., Troja, S.O., 2013. Historical mortars dating from OSL signals of fine grain fraction enriched in quartz. Geochronometria 40 (3), 153–164. http://dx.doi.org/10.2478/s13386-013-0157-y

Thomsen, K. J., Murray, A., Bøtter-Jensen, L., 2005. Sources of variability in OSL dose measurements using single grains of quartz. Radi-ation Measurements 39: 47–61, DOI 10.1016/j.radmeas.2004.01.039.

Urbanová, P., Guibert, P., 2017. Methodological study on single grain OSL dating of mortars: Comparison of five reference archaeological sites. Geochron., 44, 1, 77-97.

Urbanová, P., Hourcade, D., Ney, C., Guibert, P., 2015. Sources of uncertainties in OSL dating of archaeological mortars: the case study of the Roman amphitheatre "Palais-Gallien" in Bordeaux. Radiation Measurements, 72, 100-110.

Urbanová, P., Delaval, É., Lanos, P., Guibert, P., Dufresne, P., Ney ; C., Thernot, R., Mellinand, P., 2016. Multi-method dating of Grimaldi castle foundations in Antibes, France, ArcheoSciences, 40, 17-33.

Urbanová, P., Michel, A., Cantin, N., Guibert, P., Lanos, P., Dufresne, P., Garnier, L., 2018. A novel interdisciplinary approach for building archaeology: The integration of mortar "single grain" luminescence dating into archaeological research, the example of Saint Seurin Basilica, Bordeaux. J. Arch. Sci: Rep, 20, 307-323.

Urbanová, P., Régaldo-Saint Blancard, P., Guibert, P., Lanos, P., Hervé, G., Dufresne, P., Bouvier, A., in press. Le site paléochrétien Notre-Dame-de-la-Place à Bordeaux : nouveaux acquis chronologiques. Archéologie médiévale.

Veitch, R.J., Hedley, I.G., Wagner, J.J., 1984. An investigation of the intensity of the geomagnetic field during Roman times using magnetically anisotropic bricks and tiles. Archaeol. Sci. 359–373 Geneva.

Wintle, A. G., Murray, A. S., 2006. A review of quartz optically stimulated luminescence characteristics and their relevance in single-aliquot regeneration dating protocols. Radiation Measurements 41(4): 369–391, doi:10.1016/j.radmeas.2005.11.001.

Figure captions

Figure 1: (a) General plan of the Late Roman Antiquity urban fortification at Le Mans. (b) Plan of the sector 11 highlighting sampled walls and structures. (c) View of the sector 11 from South-East i.e., from outside the Roman walls. (d) Drawing of the section 11-300. The red arrows indicate the lowest brick course sampled for the archaeomagnetic study. (From Meunier and Monteil, 2019, 2020; CAD: H. Meunier)

Figure 2: Simplified stratigraphic diagram of studied contexts with the number of obtained dates. The diagram reproduces the formalism of Chronomodel software (Lanos and Dufresne, 2019). Rectangular boxes correspond to dated events, while circular boxes indicate *Termini Ante Quem* and *Post Quem* (called bounds in Chronomodel). The structures related to the construction of the Late Antiquity Roman wall are in red, those before the construction in blue and those posterior to the construction in green.

Figure 3: (a) In the hypothesis of a baking of the brick on one face, only one of the three possible positions provides an inclination value in agreement with the secular variation in France over the last millennia (from Lanos, 1994). (b) Orientation of the archaeomagnetic specimens within the brick and directional components of the TRM in this coordinate system.

Figure 4: Archaeomagnetic directional results. (a-c) Representative orthogonal plots with open (solid) circles being the projections upon vertical (horizontal plane). The red line shows the direction of the TRM component determined by principal component analysis. (b) Stereographic plot of TRM directions in the coordinate system of the brick after correction for TRM anisotropy. Solid and open circles correspond to positive and negative inclinations respectively. Grey shaded areas highlight range of values corresponding to the three possible positions in this coordinate

1081 system. (c) Stereographic plot of the directions after rotation in the baking position providing an
1082 inclination consistent with the secular variation (~55-75° in France).
1083
1084 Figure 5: Archaeomagnetic dating of the bricks from section 11-300 of the Late Roman Antiquity
1085 wall. The comparison of the average inclination relocated to Paris provides a probability density
1086 function, on which are defined two intervals of date at 95% of confidence.
1087
1088 Figure 6: Histogram of individual equivalent doses of quartz grains extracted from a
1089 representative lime mortar sample (BDX22214).
1090
1091 Figure 7: K-Th concentrations in OSL samples illustrating differences in internal radioactivity
1092 according to their nature.
1093
1094 Figure 8: Summary of radiocarbon, SG-OSL, OSL and archaeomagnetic dates.
1095
1096 Figure 9: Results of Bayesian chronological modelling using Chronomodel 2.0 software with the
1097 probability density function (pdf) of each event. The line above the pdf indicates the highest
1098 posterior density intervals at 95% of confidence. The events and bounds related to the
1099 construction of the Late Antiquity Roman wall are in red, those before the construction in blue
1100 and those posterior to the construction in green.
1101
1102
1103 **Table captions**
1104 Table 1: Summary of chronological data. Context: location of the sample; Dating method; Dated
1105 material or artefact; Laboratory number of the sample for physical dating techniques; Results
1106 before calibration for physical dating techniques: uncalibrated age with 1σ standard deviation for

^{14}C, age in years before year of measurement with 1σ standard deviation for OSL, average inclination with radius of the 95% confidence circle (α_{95}), precision parameter (k) and number of bricks for archaeomagnetism; Date intervals.

Table 2: SG-OSL and OSL results. Location of the sample; laboratory name of the sample; type of material; archaeological dose; annual dose; OSL age in years before the year of experiments (2019); systematic uncertainty; statistical uncertainty; total uncertainty; date with 1σ standard deviation. Uncertainties are expressed in standard deviation. Archaeological and annual dosses are rounded to the second decimal.